an increase in intracellular free Ca^{2+} concentration ($[Ca^{2+}]_i$) that consists of the following two phases: an initial transient increase and a subsequent sustained increase (1, 3 – 6). Pharmacological and electrophysiological studies using $[Ca^{2+}]_i$ measurement and whole-cell patch clamp have shown that the transient $[Ca^{2+}]_i$ increase is due to IP_3-mediated Ca^{2+} release from endoplasmic reticulum, whereas the ET-1–induced sustained $[Ca^{2+}]_i$ increase is due to Ca^{2+} influx through voltage-independent, Ca^{2+}-permeable nonselective cation channel (NSCC), which is a member of the receptor-operated Ca^{2+} channels (ROCCs) (1, 2, 4, 5), and Na^+/Ca^{2+} exchanger (NCX) operated via Na^+ influx resulting from activation of Na^+/H^+ exchanger (NHE) (7). Among G_q, G_s, and G_{12} proteins coupled with ET_AR, G_q, and G_{12} are reported to be involved in activation of NSCCs triggered by ET-1 in CHO cells expressing recombinant human ET_AR (1, 2). In contrast, ET_AR signaling cascades required for activation of NHE regulating extracellular acidification rate (ECAR) are less well characterized.

Recently, accumulating evidence from a variety of GPCRs such as calcitonin, opioid, and β-adrenergic receptors (β-ARs) has demonstrated that an agonist activating the same receptor can trigger pleiotropic effects, although the same cellular response pattern with or without differences in their potency and/or efficacy has been assumed on the basis of traditional pharmacological concepts (8 – 10). This phenomenon has been referred to by many names including "ligand-directed signaling", "agonist-directed trafficking", "biased agonism", "protean agonism", or "functional selectivity" (8, 9, 11, 12). One of the important factors giving such multiple signaling generated by stimulation of a single GPCR is the receptor expression level that affects receptor–G protein coupling in recombinant expression systems (9, 10). For example, stimulation of G_s-coupled calcitonin receptors expressed in human embryonic kidney (HEK) 293 cells at low level causes cAMP production, whereas higher level of receptor expression leads to an increase in $[Ca^{2+}]_i$ in addition to cAMP, implying that $G_{q/11}$ coupling to calcitonin receptors is dependent on their expression levels (10). Thus, excessive expression of GPCRs results in production of multiple coupling of the receptors to various G proteins, possibly due to loss of the fidelity of receptor–G protein coupling (13). It remains to be determined how the expression level of recombinant human ET_AR influences coupling of the receptors with G proteins and its downstream-signaling, although the receptor–G protein coupling depending on the receptor density can control not only the quantity of the GPCR-mediated response but also the quality of the response.

The present study examined receptor density–linked activation of signaling pathways in order to explore the multiple signaling pathways of human ET_AR. The results with CHO cells expressing ET_AR at different expression levels provide evidence that coupling of ET_AR to $G_{q/11}$ and G_{12} varies depending on the expression levels of the receptors, leading to the activation of different signaling cascades for the human ET_AR. The lack of ET_AR-G_{12} coupling results in the disappearance of sustained Ca^{2+} influx. ET_AR can utilize multiple signaling pathways including $G_{q/11}$/PLC/NHE, G_{12}/p38 mitogen–activated protein kinase (p38MAPK)/NHE, and $G_{q/11}$/PLC /p38MAPK/NHE cascades to induce the same functional response, an increase in ECAR.

Materials and Methods

Materials

YM-254890 was kindly provided by Astellas Pharma, Inc. (Tokyo). The following drugs and regents were used in the present study: synthetic human ET-1 (Peptide Institute, Osaka); fura-2/acetoxymethyl ester (fura-2 /AM), fluo-3/AM, Pluronic F-127 (Dojindo Laboratories, Kumamoto); SB203580 hydrochloride [4-(4-fluorophenyl)-2-(4-methylsulfinyl phenyl)-5-(4-pyridyl) 1*H*-imidazole hydrochloride], 2',5'-dideoxyadenosine, NF449 {4,4',4",4"'-[carbonyl-bis[imino-5,1,3-benzene-triylbis-(carbonylimino)]]tetrakis-(benzene-1,3-disulfonate}, U-73122 {1-[6-((17β-3-methoxyestra-1,3,5(10)-trien-17-yl)amino)hexyl]-1*H*-pyrrole-2,5-dione} (Calbiochem, San Diego, CA, USA); PD142893 (*N*-acetyl-β-phenyl-D-Phe-Leu-Asp-Ile-Ile-Trp), EIPA [5-(*N*-ethyl-*N*-isopropyl)amiloride], probenecid, aprotinin, leupeptin, pepstatin, sodium deoxycholate, sodium dodecyl sulfate (SDS), phenylmethylsulfonyl fluoride (PMSF), Na_3VO_4, NaF, puromycin dihydrochloride (Sigma-Aldrich Co., St. Louis, MO, USA); [^{3}H]BQ123 {cyclo-(D-Trp-D-Asp-[prolyl-3,4(*n*)-^{3}H]-D-Val-Leu), specific activity: 18.0 Ci/mmol} (Amersham Biosciences, Amersham Place Little Chalfont, Buckinghamshire, UK). All cell culture media and supplements except fetal calf serum (FCS; Invitrogen Corp., Grand Island, NY, USA) were obtained from Sigma-Aldrich. Antibodies were obtained from Cell Signaling Technology, Inc. (Beverly, MA, USA). The other regents used were of the highest grade in purity.

Cell culture

CHO cells were grown as monolayers cultured in Ham's F-12 medium supplemented with 10% ($v \cdot v^{-1}$) FCS, penicillin (100 units $\cdot$ ml^{-1}), and streptomycin (100 μg $\cdot$ ml^{-1}) at 37°C in humidified air with 5% CO_2.

Stable expression of human ET_AR in CHO cells

The gene of human ET_AR fused with yellow fluorescence protein (YFP) at the C terminus was introduced into CHO cells by retroviral gene transfer as previously described (6). The cells were grown for 48 h and then stable transformants were selected in medium containing 5 $\mu g \cdot ml^{-1}$ puromycin for a week. The cells were sorted into eight populations by using flow cytometry (FACSVantage™; BD Biosciences, San Jose, CA, USA) based on their YFP fluorescence intensity. Clonal cell lines were obtained by limiting dilution of each cell population. Clones were expanded and screened for expression levels by radioligand binding analyses with a single concentration of [^{3}H]BQ-123 (2 nM). Suitable clones were grown up for a full saturation binding assay.

Whole-cell binding assay

Saturation binding assay was conducted with intact cells using the radioligand [^{3}H]BQ-123. CHO cells expressing human ET_AR at different expression level were washed twice and harvested with 0.02% EDTA in phosphate-buffered saline (PBS; pH 7.4) by gentle pipetting. The resulting cell pellets were washed once and resuspended in Ca^{2+}-free Krebs-HEPES solution (140 mM NaCl, 3 mM KCl, 1 mM $MgCl_2 \cdot 6H_2O$, 11 mM D-(+)-glucose, 10 mM HEPES; adjusted to pH 7.3 with NaOH) at $1 - 5 \times 10^6$ cells/ml. Intact cells were incubated in 500 μl of Ca^{2+}-free Krebs-HEPES solution containing 0.1% bovine serum albumin (BSA) with [^{3}H]BQ-123 at concentrations ranging 0.1 – 5 nM at 4°C for 24 h. To avoid radioligand depletion, cell number in each incubation tube was adjusted to 0.5 – 2.5×10^5 cells, depending on their receptor expression levels. Nonspecific binding was defined by the presence of 1 μM PD142893, a nonselective ET_AR and ET_BR antagonist (14). Assays were terminated by rapid filtration using a Brandel cell harvester (Brandel, Inc., Gaithersburg, MD, USA) over Whatman GF/C filters presoaked with 0.3% polyethyleneimine for 60 min. The filters were rapidly washed 3× with 5-ml aliquots of ice-cold washing buffer (50 mM Tris-HCl, pH 7.4), and dried before the measurement of filter-bound radioactivity. The radioactivity was counted in a liquid scintillation counter (LC-3500; Aloka, Tokyo) using a scintillation fluid (Clear-sol II; Nacalai Tesque, Kyoto). The protein contents were determined by the method of Bradford (15) using BSA as standard.

Measurement of ECAR

The eight-channel Cytosensor™ microphysiometer (Molecular Devices Corp., Sunnyvale, CA, USA) was used to measure ET_AR-mediated changes in ECAR. Briefly, CHO cells expressing ET_AR were seeded into 12-mm capsule cups at density of 5×10^5 cells per cup and cultured in Ham's F-12 medium supplemented with 0.5% FCS at 37°C in an atmosphere of 5% CO_2 for 24 h. On the day of the experiment, the capsule cups were loaded into the sensor chambers of the instrument, and the chambers were perfused with running medium, which was modified RPMI-1640 (Molecular Devices Corp.) containing 0.1% BSA, at a flow rate of 100 $\mu l \cdot min^{-1}$. During a 2-min pump cycle, the pump was on for 1 min 20 s and then switched off for the remaining 40 s. The ECAR was measured from 1:28 to 1:58 min in every cycle. The paired sister cells were equilibrated for 90 min and then were treated with either vehicle [0.2% dimethylsulfoxide (DMSO)] or inhibitors for 30 min before stimulation with ET-1 for 30 min. Final DMSO concentration in the medium did not affect the ECAR responses to ET-1 (data not shown). All drugs were diluted into running medium and perfused through either fluid path. Results are expressed as a % of the basal ECAR prior to exposure to DMSO or inhibitor.

Adenovirus infection

Recombinant adenoviruses encoding green fluorescence protein (GFP) and the C-terminus region of $G_{\alpha 12}$ protein ($G_{\alpha 12}$-ct) along with GFP protein (16) were kindly provided by Dr. Hitoshi Kurose (Kyushu University, Fukuoka). CHO cells grown to 100% confluence in six-well plates at a density of approximately 3×10^6 cells/well were infected by recombinant adenovirus for 2 h at 300 multiplicity of infection (MOI). After infection, the cells were cultured in Ham's F-12 medium containing 0.5% FCS for 60 h. Subsequently, the cells were maintained for 12 h in the absence of FCS for Western blot analysis. To estimate the efficiency of adenoviral infection in CHO cells, expression level of recombinant protein GFP was determined by flow cytometry analysis.

Flow cytometry analysis

CHO cells with or without adenovirus infection grown in six-well plates were harvested with 0.02% EDTA in PBS and then resuspended in PBS containing 1% FCS and 0.01% NaN_3. The cell suspensions were analyzed on a FACSCalibur™ flow cytometer (BD Biosciences) using CellQuest software (BD Biosciences).

Detection of mRNA for $G_{\alpha 12}$-ct by reverse transcription–polymerase chain reaction (RT-PCR)

Total RNA was isolated from CHO cells infected by recombinant adenovirus encoding GFP or $G_{\alpha 12}$-ct along with GFP using an RNeasy Kit (QIAGEN K.K., Tokyo) according to the manufacturer's protocol. The isolated RNA was reverse transcribed using the SuperScript™

First-Strand Synthesis System Kit (Invitrogen), and the resultant first-strand cDNA was applied to PCR, which was performed using a HotStarTaq™ Master Mix Kit (QIAGEN K.K.). A negative control without reverse transcriptase was run in parallel to verify that amplification did not proceed from residual genomic DNA. The sequences of the forward and reverse primers were 5'-GATCCGCTAGAGATCTGGTACCATG-3' and 5'-CTGCAGCATGATGTCTTTCAGGTTC-3', respectively (16). cDNA was heated for 15 min at 95°C and then amplified by 35 cycles (95°C for 30 s, 55°C for 30 s, 72°C for 30 s) followed by 5 min of extension at 72°C. The PCR products were confirmed by a single band on electrophoresis with 2.0% ethidium bromide–stained agarose gels.

Measurement of $[Ca^{2+}]_i$

$[Ca^{2+}]_i$ was monitored by using a fluorescent Ca^{2+} indicator, fura-2/AM, as described previously (6, 17). In the experiments using SB203580 and EIPA, $[Ca^{2+}]_i$ was measured using fluo-3 (excitation = 490 nm, emission = 540 nm) instead of fura-2, because addition of these inhibitors was found to interfere with fluorescence signals of fura-2 (data not shown).

Western blot analysis

Cells grown in six-well plates were serum-starved for 12 h before drug treatment. After the various treatments, cells were washed with ice-cold PBS, and collected into lysis buffer (150 mM NaCl, 1.5 mM $MgCl_2$, 50 mM Tris-HCl (pH 6.8), 1% NP-40, 0.5% sodium deoxycholate, 0.1% SDS, 1 mM PMSF, 1 mM Na_3VO_4, 20 mM NaF, 10 $\mu g \cdot ml^{-1}$ leupeptin, 10 $\mu g \cdot ml^{-1}$ aprotinin, and 10 $\mu g \cdot ml^{-1}$ pepstatin) supplemented with EDTA-free, protease inhibitor cocktail (PIERCE Biotechnology, Inc., Rockford, IL, USA). The cell lysates were sonicated for 10 s and centrifuged at 15,000 rpm for 10 min at 4°C. The resulting supernatants were combined with SDS sample buffer [62.5 mM Tris-HCl (pH 6.8), 10% glycerol, 5% 2-mercaptoethanol (2-ME), 2.5% SDS, 0.1% bromphenol blue] followed by heating to 100°C for 5 min. The samples were separated on a 12.5% polyacrylamide gel (SuperSep™; Wako Pure Chemical Industries, Ltd., Osaka) and electrotransferred to a polyvinylidene fluoride membrane (Immobilon™-P, pore size 0.45 μm; Millipore Corp., Bedford, MA, USA) with a semi-dry electroblotter. After transfer, the membranes were washed with Tris-buffered saline-Tween 20 [TBST: 10 mM Tris-HCl (pH 8.0), 100 mM NaCl, and 1% Tween-20] for 5 min followed by blocking (5% non-fat dry milk in TBST) of nonspecific binding for 1 h at room temperature. The membranes were incubated with a phospho-p38MAPK (Thr180/Tyr182) antibody as a primary antibody overnight at 4°C. The primary antibody was detected with a secondary horseradish peroxidase–conjugated anti-rabbit IgG antibody and enhanced chemiluminescence (ECL, Amersham Biosciences). The membranes were then stripped with stripping buffer [62.5 mM Tris-HCl (pH 7.0), 2% SDS, 1% 2-ME] for 1 h at 50°C and reprobed with a p38MAPK antibody, detected with the same secondary antibody. The blots were exposed to Amersham Hyperfilm™ ECL (GE Healthcare Limited, Little Chalfont, Buckinghamshire, UK). Optical density on the film was analyzed with National Institutes of Health Image J1.37 software. p38MAPK phosphorylation was routinely expressed as the ratio of phosphorylated p38MAPK to total p38MAPK.

Data analyses

Data regarding ECAR and $[Ca^{2+}]_i$ were collected and analyzed by using the Cytosoft™ (Molecular Devices Corp.) and a MacLab/8s with Chart (v. 3.5) software (ADInstruments Japan, Tokyo), respectively. The concentration–response curves for ET-1 were constructed to evaluate its EC_{50} value, which is the effective ET-1 concentration (M) eliciting a half-maximal response using GraphPad PRISM™ (version 3.00; GraphPad Software, Inc., San Diego, CA, USA). The EC_{50} values were converted to negative logarithmic values (pEC_{50}) for analysis. Saturation binding data were analyzed by non-linear regression using GraphPad PRISM™. The computer software provides equilibrium dissociation constants (K_D) and maximum number of binding sites (B_{max}) from saturation curves. Abundance of ET_AR in CHO cells was represented as the binding capacity per milligram of protein for each (B_{max}: femtomoles per milligram of protein). All data are presented as means ± S.E.M. where n refers to the number of experiments. The significance of the difference between mean values was evaluated with GraphPad PRISM™ by Student's paired *t*-test, unpaired *t*-test, or one-way analysis of variance (ANOVA) followed by Tukey's multiple comparison test. A *P* value less than 0.05 was considered to indicate a significant difference.

Results

Radioligand binding experiments

Eighteen stable cell lines obtained by limiting dilution showed different expression levels of human ET_AR ranging from 32,100 ± 5,913 (ET_AR-high-CHO; n = 4, Fig. 1A) to 893 ± 66 (ET_AR-low-CHO; n = 4, Fig. 1B) fmol · mg protein^{-1} as measured with saturation binding assays. The two cell lines, designated as ET_AR-high-CHO and ET_AR-low-CHO, were used for analyzing

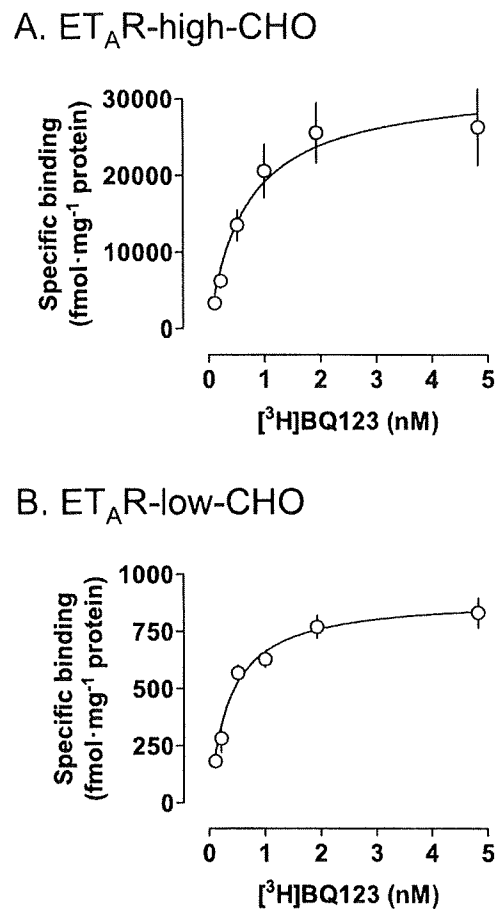

Fig. 1. Saturation binding experiments with [^{3}H]BQ123 (0.1 – 5 nM) in ET_AR-high-CHO (A) and ET_AR-low-CHO (B) using the whole-cell binding assay. Nonspecific binding was determined in the presence of PD142893 (1 μM). Each point represents the mean ± S.E.M. of 4 experiments. When no error bar is shown, the error is smaller than the symbol.

ET_AR signaling, since there was a marked difference between both cell lines in Ca^{2+} responses to ET-1, as described later. The pK_D values of ET_AR-high-CHO and ET_AR-low-CHO were 9.2 ± 0.1 (n = 4) and 9.5 ± 0.1 (n = 4), respectively. The comparable pK_D values for both groups indicated that the differences in receptor expression level had little or no effect on [^{3}H]BQ123 binding affinity for ET_AR.

Characterization of ET-1–induced increases in $[Ca^{2+}]_i$

We determined concentration–response curves for ET-1–induced increases in $[Ca^{2+}]_i$ in ET_AR-high-CHO and ET_AR-low-CHO. In wild-type CHO cells (not transfected ET_AR), ET-1 at concentrations up to 10 nM did not show any effect on $[Ca^{2+}]_i$ (data not shown), suggesting that the ET-1–induced Ca^{2+} mobilization was solely mediated by recombinant ET_AR.

In ET_AR-high-CHO, ET-1 began to induce a transient increase in $[Ca^{2+}]_i$ at 0.01 nM, which reached the maximum level at 0.3 nM, with an EC_{50} value of around 0.01 nM (Fig. 2A). Notably, the sustained increase began to appear at 0.01 nM, reached the maximum level at 0.3 nM, and remained at the similar level up to the concentration of 10 nM: the EC_{50} value was around 0.2 nM. The biphasic $[Ca^{2+}]_i$ responses consisting of transient and sustained increases were observed in other cell lines expressing ET_AR at levels over 2,700 fmol · mg protein^{-1} (Table 1). The maximum increases in $[Ca^{2+}]_i$ by ET-1 and its pEC_{50} values are summarized in Table 1.

In contrast, in ET_AR-low-CHO, ET-1 began to induce a transient increase in $[Ca^{2+}]_i$ at 0.03 nM, which was not accompanied by a sustained phase (Fig. 2B). The transient increase reached the maximum level at 3 nM, with an EC_{50} value of around 0.3 nM (Table 1). Notably, the sustained increase in $[Ca^{2+}]_i$ was very small throughout the tested concentrations of ET-1 (Fig. 2B).

The difference in sustained Ca^{2+} responses between these cell lines suggested that discrete intracellular signaling(s) is involved in development of the sustained phase triggered by ET-1, which is independent of the transient Ca^{2+} responses. To determine the influence of receptor expression levels on ET_AR signaling, subsequent experiments focused on the responses to ET-1 at 0.3 nM and 3 nM for ET_AR-high-CHO and ET_AR-low-CHO, respectively.

Determination of signaling molecules involved in the sustained increases in $[Ca^{2+}]_i$ induced by ET-1 in ET_AR-high-CHO

Stimulation of ET_AR with ET-1 is well known to elicit an increase in $[Ca^{2+}]_i$ via α-subunits derived from G_q protein (2). To confirm involvement of G_q protein in the ET-1–induced sustained increases in $[Ca^{2+}]_i$ in ET_AR-high-CHO, YM-254890, a novel $G_{\alpha q/11}$ inhibitor (18), was added during the sustained phase after stimulation of ET_AR with 0.3 nM ET-1. As shown in Fig. 3, 1 μM YM-254890 markedly inhibited the ET-1–induced sustained increases in $[Ca^{2+}]_i$, indicating that the sustained Ca^{2+} responses to ET-1 are mediated via $G_{\alpha q/11}$, as reported previously (6).

The principal downstream effector for $G_{\alpha q/11}$ is PLCβ that cleaves the membrane lipid phosphatidylinositiol-4,5-bisphosphate (PIP_2) into the second messengers such as IP_3 and DAG, both of which modulate $[Ca^{2+}]_i$ (19). In ET_AR-high-CHO, U-73122, a PLC inhibitor (6, 17), at the concentration of 3 μM significantly inhibited the ET-1–induced sustained $[Ca^{2+}]_i$ increase (Fig. 3). This result suggested that the Ca^{2+} mobilization activated by ET-1 depends on PLC activation.

An NHE-dependent mechanism is also reported to be involved in an increase in $[Ca^{2+}]_i$ triggered by stimula-

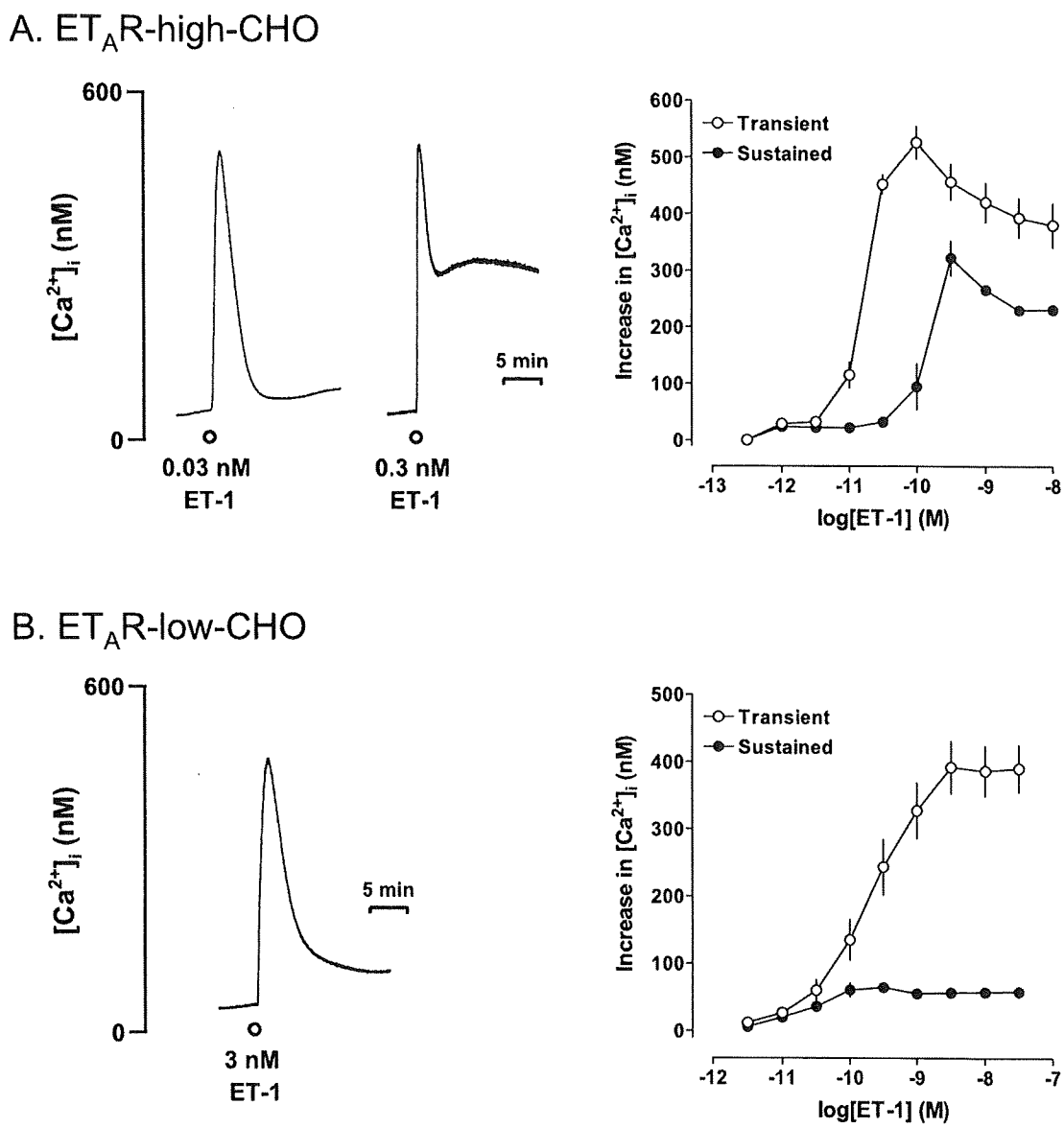

Fig. 2. Characterization of the ET-1–induced increase in $[Ca^{2+}]_i$ in ET_AR-high-CHO (A) and ET_AR-low-CHO (B). Left panels: representative traces showing the $[Ca^{2+}]_i$ increases induced by ET-1 at the indicated concentrations in ET_AR-high-CHO and ET_AR-low-CHO. Right panels: concentration–response curves for the ET-1–induced transient and sustained $[Ca^{2+}]_i$ increases. Data are presented as means ± S.E.M. of the results obtained from 5 experiments.

tion of ET_AR (7). That is, ET-1 activates NHE, causing an increase in the intracellular Na^+ concentration ($[Na^+]_i$) that in turn drives NCX operating in the reverse mode to transport Ca^{2+} into cells in exchange for Na^+ efflux, leading to an increase in $[Ca^{2+}]_i$. As indicated previously (7), pretreatment of the cells with 10 μM EIPA, a selective NHE1 inhibitor (20), partly inhibited the ET-1–induced sustained increase in $[Ca^{2+}]_i$ to 46.2 ± 2.2% (Fig. 3).

There is accumulating evidence that p38MAPK plays a functional role in ET-1–induced responses such as vascular smooth muscle contractions (21, 22). In addition, p38MAPK is a major activator of NHE (9). To clarify possible involvement of p38MAPK in Ca^{2+} responses to ET-1 in ET_AR-high-CHO, the effect of SB203580, a p38MAPK inhibitor, was examined. SB203580 inhibited the sustained increases in $[Ca^{2+}]_i$ elicited by ET-1 in a concentration-dependent manner (Fig. 3), indicating that p38MAPK also contributes to generation of the sustained Ca^{2+} influx.

Functional analysis of ET_AR signaling involved in ECAR response to ET-1 using Cytosensor™

To further analyze signaling pathways activated by

Table 1. Comparison of potencies for ET-1 on human ET_AR expressed at different levels in CHO cells estimated by $[Ca^{2+}]_i$ measurements

Expression level (fmol · mg protein^{-1})	n	Transient phase		Sustained phase	
		pEC_{50}	$[Ca^{2+}]_{iMAX}$ (nM)	pEC_{50}	$[Ca^{2+}]_{iMAX}$ (nM)
32,100 (ET_AR-high-CHO)	5	10.89 ± 0.05	525.7 ± 28.6	10.05 ± 0.09	321.9 ± 30.5
4,532	5	10.48 ± 0.01	506.4 ± 25.9	9.47 ± 0.09	289.8 ± 16.9
2,700	4	10.51 ± 0.03	639.2 ± 30.9	9.31 ± 0.03	359.6 ± 19.9
893 (ET_AR-low-CHO)	5	9.57 ± 0.03	391.7 ± 39.2	Not determined[a]	64.5 ± 5.5[a]

Results are presented as means ± S.E.M. of n number of experiments. The pEC_{50} value is the negative logarithm of the effective ET-1 concentration (M) that produces a 50% response of the maximum response, $[Ca^{2+}]_{iMAX}$. [a]Residual component of $[Ca^{2+}]_i$ after transient increase in $[Ca^{2+}]_i$ induced by ET-1, since a significant sustained phase was not generated in ET_AR-low-CHO.

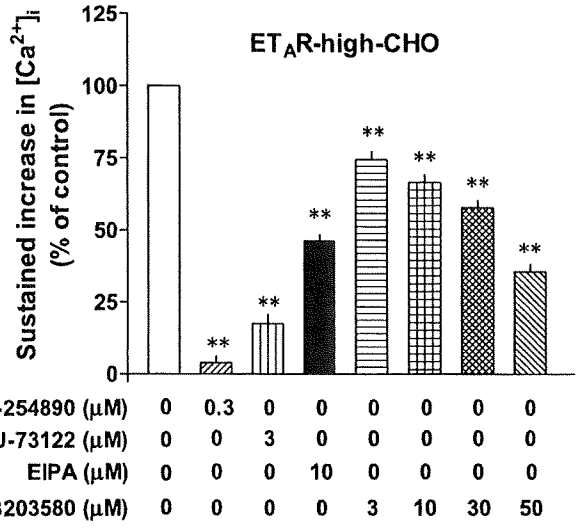

Fig. 3. Effects of YM-254890, U-73122, EIPA, and SB203580 on the sustained increases in $[Ca^{2+}]_i$ induced by 0.3 nM ET-1 in ET_AR-high-CHO. These inhibitors were added during the sustained phase after stimulation with ET-1. The $[Ca^{2+}]_i$ level induced by 0.3 nM ET-1 before addition of the inhibitors was set to 100% as a control. Data are presented as means ± S.E.M. of the results obtained from 4 – 6 experiments. $^{**}P<0.01$, vs. its control (0.3 nM ET-1 alone, open column).

ET_AR, the change in ECAR was continuously measured every 2 min by using the Cytosensor™ microphysiometer that allows the analysis of signaling molecules activated by GPCRs in living cells (23).

In ET_AR-high-CHO, 0.3 nM ET-1 induced an increase in ECAR (Fig. 4A). The ECAR response to ET-1 was completely inhibited by 10 μM EIPA, indicating the predominant role of NHE1 in the ECAR responses. To elucidate upstream signaling cascades in activation of NHE1, the effects of YM-254890, U-73122, and SB203580 on the increase in ECAR response to ET-1 were examined. Surprisingly, the sensitivity of the ECAR response to these inhibitors changed appreciably with time in ET_AR-high-CHO (Fig. 4A). Unlike the Ca^{2+} response to ET-1, the early ECAR response to ET-1 (e.g., at 2 min after ET-1 stimulation) was sensitive to either 1 μM YM-254890 or 10 μM U-73122, but insensitive to 50 μM SB203580. In contrast, the late ECAR response (e.g., at 30 min) was resistant to both YM-254890 and U-73122, whereas it was sensitive to SB203580 (Fig. 4A). These findings raised the interesting possibility that a major contributor to the ET-1–induced ECAR response in ET_AR-high-CHO varies with time from the $G_{\alpha q/11}$/PLC-dependent, p38MAPK-independent pathway to the $G_{\alpha q/11}$/PLC-independent, p38MAPK-dependent pathway.

In contrast to ET_AR-high-CHO, the increases in ECAR induced by ET-1 in ET_AR-low-CHO were sensitive to all inhibitors mentioned above until 30 min after ET-1 addition (Fig. 4B), implying the involvement of $G_{\alpha q/11}$, PLC, and p38MAPK in the ECAR response to ET-1.

It is reported that ET_AR is able to couple with G_s protein in addition to G_q and G_{12} proteins (1, 2). Activation of AC by stimulation of G_s protein–coupled β_3-ARs is reported to result in an increase in ECAR (9). However, possible involvement of the G_s/AC pathway in the ET_AR-mediated ECAR response can be ruled out, since NF449 (100 μM), a G_s inhibitor (24), and 2',5'-dideoxyadenosine (50 μM), an AC inhibitor (9), had no inhibitory effect on the ET-1–induced change in ECAR in ET_AR-high-CHO and ET_AR-low-CHO (data not shown).

Characterization of ET-1–induced phosphorylation of p38 MAPK

To confirm the involvement of p38MAPK in the ET_AR signaling, phosphorylation levels of p38MAPK was estimated by Western blot analysis. ET-1 at concentrations of 0.3 and 3 nM induced phosphorylation of p38MAPK in ET_AR-high-CHO and ET_AR-low-CHO, respectively, and the maximum phosphorylation responses were maintained up to 10 min (Fig. 5A). Treatment of both cell lines with ET-1 elicited phosphorylation of p38MAPK in a concentration-dependent manner with pEC_{50} values of 10.16 ± 0.21 and 9.64 ±

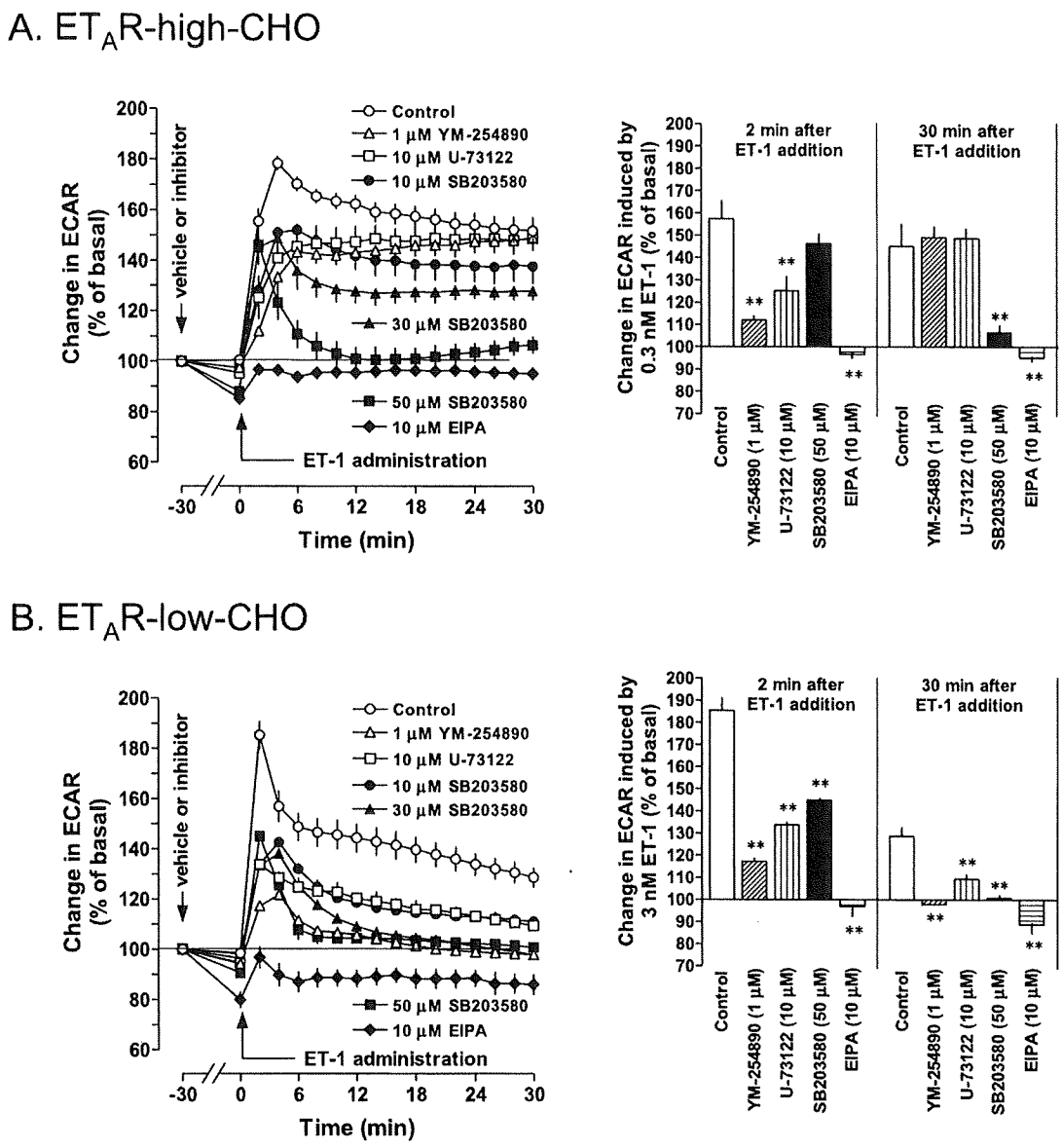

Fig. 4. Characterization of changes in ECAR induced by 0.3 nM ET-1 in ET_AR-high-CHO (A) and by 3 nM ET-1 in ET_AR-low-CHO (B). The change in ECAR was measured by the Cytosensor™ microphysiometer every 2 min. The cells were treated with either vehicle (0.2% DMSO) or inhibitor for 30 min before stimulation with ET-1 (ET-1 administration) for 30 min. Effects of YM-254890, U-73122, SB203580, and EIPA on the ECAR response to ET-1 at 2 and 10 min are shown in the right panel. Data are presented as means ± S.E.M. of the results obtained from 4 – 6 experiments. $^{**}P<0.01$, vs. its control (ET-1 alone, open column).

0.23, respectively, which reached the maximum levels of 971.6 ± 50.8% and 591.3 ± 80.7%, respectively (Fig. 5B).

To determine upstream regulatory molecules for p38MAPK, the effects of inhibitors for $G_{\alpha q/11}$ and PLC on the ET-1–induced phosphorylation of p38MAPK were examined. YM-254890 (1 μM) had little or no effect on the p38MAPK phosphorylation by ET-1 in ET_AR-high-CHO (Fig. 6A), whereas it significantly inhibited the phosphorylation in ET_AR-low-CHO (Fig. 6B). U-73122 (10 μM) itself increased phosphorylation of p38MAPK. In the presence of U-73122 (10 μM), ET-1 still caused phosphorylation of p38MAPK in ET_AR-high-CHO (Fig. 6A). In contrast, ET-1 failed to induce a further increase in p38MAPK phosphorylation in ET_AR-low-CHO treated with U-73122 (Fig. 6B). These results suggested that activation of p38MAPK after ET-1 treatment was predominantly mediated via the non-$G_{\alpha q/11}$/PLC pathway in ET_AR-high-CHO but the $G_{\alpha q/11}$/PLC pathway in ET_AR-low-CHO.

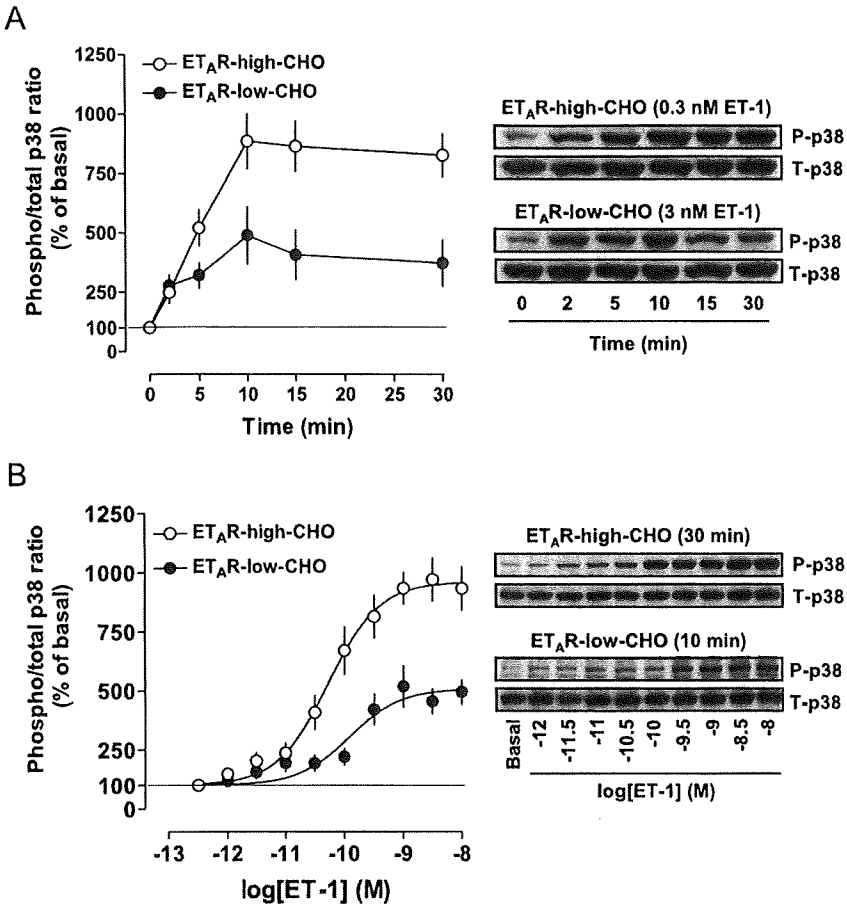

Fig. 5. Characterization of p38MAPK phosphorylation in response to ET-1 in ET_AR-high-CHO and ET_AR-low-CHO. A) Time course of p38MAPK phosphorylation induced by 0.3 nM ET-1 in ET_AR-high-CHO and by 3 nM in ET-1 in ET_AR-low-CHO with, at the right, representative immunoblots (P-p38, phosphorylated p38MAPK; T-p38, total p38MAPK). B) Concentration–response curves for p38MAPK phosphorylation in response to 30- and 10-min exposure to ET-1 in ET_AR-high-CHO and ET_AR-low-CHO, respectively, with, at the right, representative immunoblots. Data are presented as means ± S.E.M. of the results obtained from 6 experiments.

To elucidate $G_{\alpha q/11}$/PLC-independent pathways contributing to the ET-1–induced phosphorylation of p38MAPK in ET_AR-high-CHO, the possible involvement of $G_{\alpha 12}$ protein was examined using recombinant adenovirus that introduces $G_{\alpha 12}$-ct along with GFP protein into cells. Adenovirus infection at 300 MOI of CHO cells expressing ET_AR resulted in expression of recombinant GFP in approximately 90% of cells, as determined by fluorescence of GFP with flow cytometry (Fig. 7). mRNA expression for $G_{\alpha 12}$-ct was assessed by RT-PCR in either ET_AR-high-CHO or ET_AR-low-CHO after infection of recombinant adenovirus encoding $G_{\alpha 12}$-ct but not GFP (Fig. 8). Furthermore, no band corresponding to $G_{\alpha 12}$-ct was present in the PCR products without RT (data not shown). These results rule out the possibility that these fragments are non-specifically amplified products derived from contaminating genomic DNA. The effects of $G_{\alpha 12}$-ct on the ET-1–induced phosphorylation of p38MAPK were assessed by comparing the responses in GFP-expressing cells with those in $G_{\alpha 12}$-ct-expressing cells, since the $G_{\alpha 12}$-ct construct also expresses GFP (16).

The expression of $G_{\alpha 12}$-ct by adenovirus infection did not affect basal levels of p38MAPK phosphorylation in the absence of ET-1 stimulation, in either ET_AR-high-CHO or ET_AR-low-CHO. In contrast, the expression of $G_{\alpha 12}$-ct significantly inhibited the ET-1–evoked increases in levels of p38MAPK phosphorylation in ET_AR-high-CHO (Fig. 9A) but not in ET_AR-low-CHO (Fig. 9B). These results suggest that receptor-G_{12} coupling is required for activation of p38MAPK by ET-1 in ET_AR-high-CHO.

Discussion

There is considerable evidence that receptor expression level is an important determinant for coupling of receptor with G proteins. In recombinant systems, promiscuous interaction of receptors with G proteins was observed, when receptor density increased. It has been reported that G_s and G_q coupling to calcitonin receptors expressed in HEK293 cells (10) and G_i and G_s coupling to α_2-ARs expressed in CHO cells (25) are dependent on the receptor expression level. Such multiple coupling of receptors to G proteins is speculated to induce differential cellular responses to an agonist acting on the same receptor. The present study compared the signal transduction pathways utilized by human ET_AR expressed in

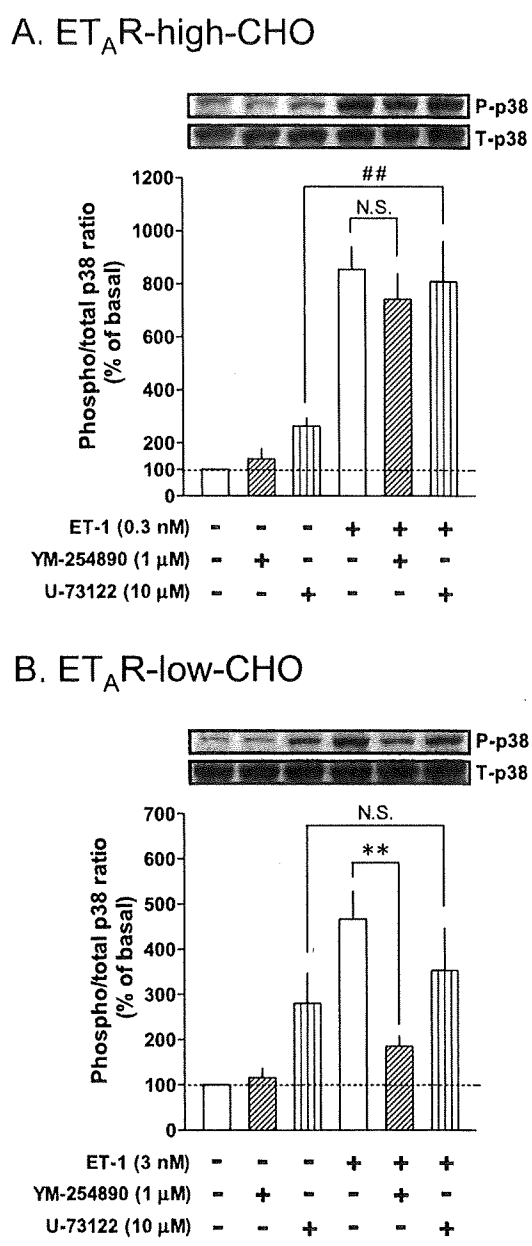

Fig. 6. Effects of YM-254890 and U-73122 on p38MAPK phosphorylation in response to 30-min exposure to 0.3 nM ET-1 in ET_AR-high-CHO (A) and to 10 min exposure to 3 nM ET-1 in ET_AR-low-CHO (B). The cells were treated with the inhibitors for 30 min before stimulation with ET-1. Data are presented as means ± S.E.M. of the results obtained from 6 experiments. $^{\#\#}P<0.01$, between both groups indicated. $^{**}P<0.01$, vs. its control (3 nM ET-1 alone). N.S., not significant between the indicated columns.

CHO cells at different levels (referred to as ET_AR-high-CHO and ET_AR-low-CHO in this paper) to clarify the functional significance of receptor density in determining the coupling of ET_AR to G_q and G_{12} proteins and its down-stream signaling cascades.

The potency of ET-1 in inducing transient $[Ca^{2+}]_i$ increases was approximately 20-fold higher in ET_AR-high-CHO than in ET_AR-low-CHO, although the binding affinity of [^{3}H]BQ123 for ET_AR in both cell lines was similar to each other. This finding clearly indicates that an increase in ET_AR expression level leads to changes in the efficacy of ET-1. Alternations in agonist potency or efficacy are reported to be frequently accompanied by activation of multiple signaling pathways (26).

In ET_AR-high-CHO, high concentrations of ET-1 induced an increase in $[Ca^{2+}]_i$ consisting of two phases, a transient phase and a subsequent sustained phase, as reported previously (6). It is generally thought that the initial Ca^{2+} signal phase (produced by G_q protein–coupled receptors) is generated by IP_3-dependent Ca^{2+} release from the intracellular Ca^{2+} store and that the resulting depletion of the Ca^{2+} store triggers activation of store-operated Ca^{2+} channels (SOCCs), leading to the sustained $[Ca^{2+}]_i$ increase (27, 28). However, such a scheme in which development of ET-1–induced sustained phase is dependent on its initial $[Ca^{2+}]_i$ increase cannot provide an entirely satisfactory explanation for our results obtained in ET_AR-high-CHO and ET_AR-low-CHO, since the amplitude of sustained Ca^{2+} influx evoked by ET-1was not correlated with that of the initial increases in $[Ca^{2+}]_i$. That is, although the transient $[Ca^{2+}]_i$ increases induced by 0.3 nM ET-1 in ET_AR-high-CHO and by 3 nM ET-1 in ET_AR-low-CHO are comparable with each other (Fig. 2), the amplitude of the sustained Ca^{2+} responses to ET-1 was markedly different in these two types of cells. These findings suggest that the ET-1–induced sustained Ca^{2+} influx in ET_AR-high-CHO is not due to SOCCs operated by the emptying of the intracellular Ca^{2+} store (29, 30). Key candidates for such SOCC-independent pathways are NSCCs (1) and NHE (7), both of which are reported to be activated by GPCRs. Regarding NSCCs, it has been suggested that both G_q and G_{12} proteins are necessary for activation of these channels by ET_AR in CHO cells overexpressing ET_AR, although the receptor density of the cells is not determined (1, 2). In ET_AR-high-CHO and ET_AR-low-CHO, ET_AR is considered to be coupled with $G_{q/11}$ protein, judging from the sensitivity of the ET-1–induced transient increases of $[Ca^{2+}]_i$ in both cell lines to a $G_{\alpha q/11}$ inhibitor (YM-254890) and a PLC inhibitor (U-73122) (data not shown) and from the sensitivity of the sustained increases in ET_AR-high-CHO to these inhibitors (Fig. 3). Based on these data, we assumed that the difference of sustained Ca^{2+} influx in ET_AR-high-CHO and ET_AR-low-CHO is due to different efficiency of coupling of ET_AR to G_{12} protein, which in turn depends on the expression level of ET_AR. Namely, in ET_AR-low-CHO, ET-1 could not activate G_{12}-mediated signaling pathways, failing to induce sustained Ca^{2+}

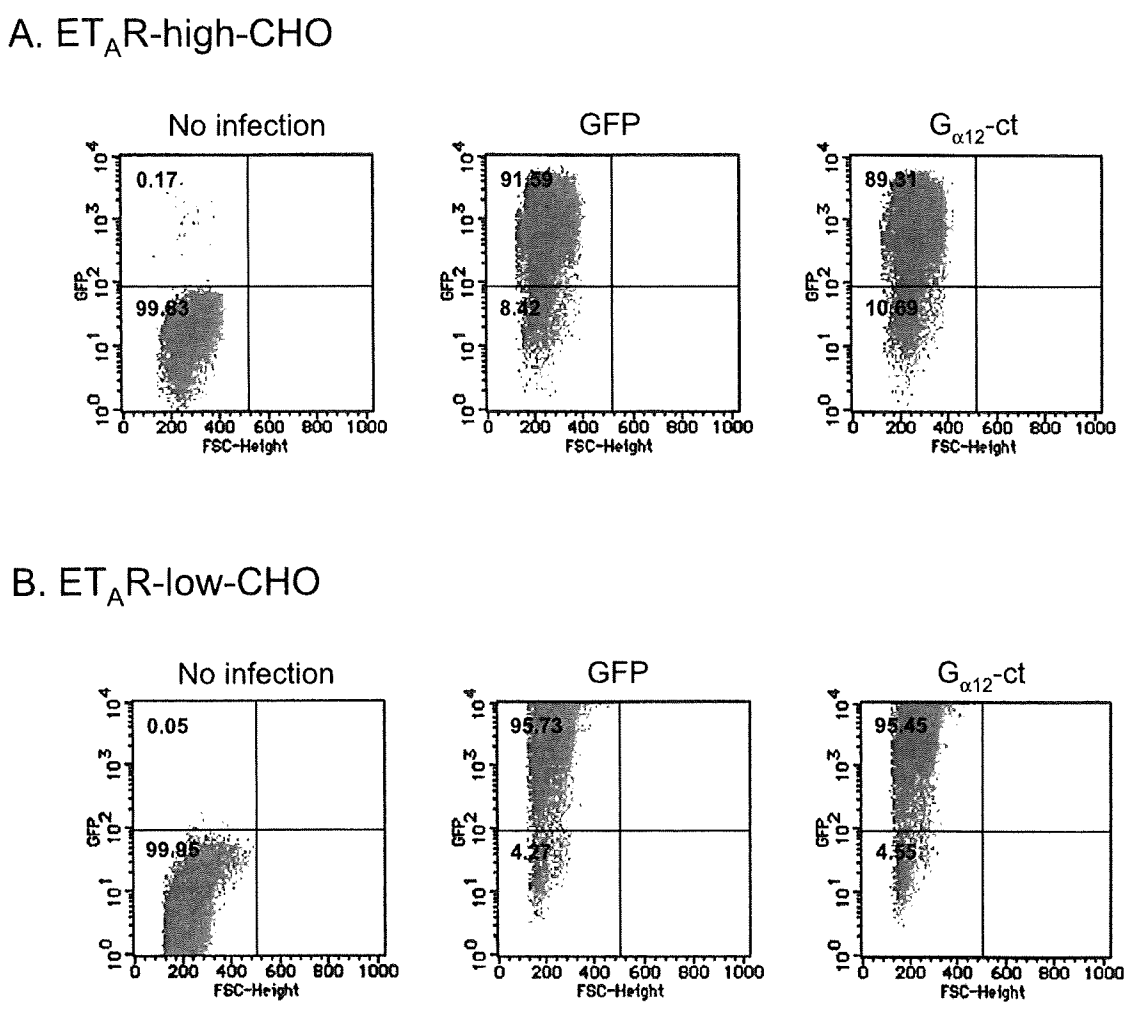

Fig. 7. The efficiency of adenoviral infection at 300 MOI in ET_AR-high-CHO (A) and ET_AR-low-CHO (B) determined by detecting fluorescence of GFP with flow cytometry. Numbers in the left lower and upper quadrants indicate the percentages of GFP-negative and -positive cells, respectively.

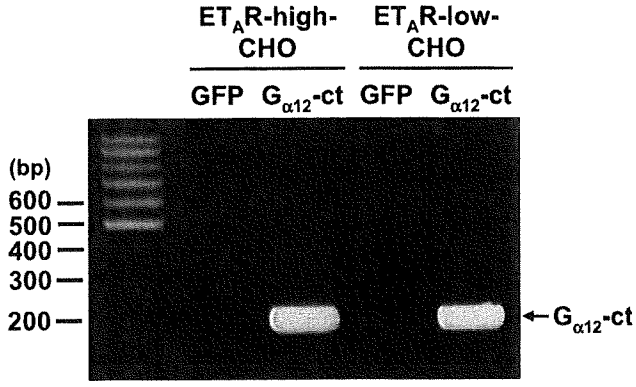

Fig. 8. Detection by RT-PCR of $G_{\alpha 12}$-ct mRNA in ET_AR-high-CHO and ET_AR-low-CHO infected by adenovirus encoding GFP or $G_{\alpha 12}$-ct. RT-PCR experiments were carried out using total RNA prepared from 3 individual cell populations. Left lane shows a 100-bp DNA ladder (Promega, Madison, WI, USA).

influx in cooperation with $G_{q/11}$-mediated signaling pathways. Furthermore, the ET-1–induced sustained increases in $[Ca^{2+}]_i$ in ET_AR-high-CHO was attenuated by inhibitors of either NHE (EIPA) or p38MAPK (SB203580) (Fig. 3). p38MAPK is reported to play a central role in the activation of NHE (9). These data implicate the involvement of the p38MAPK/NHE pathway in the sustained Ca^{2+} response to ET-1 in ET_AR-high-CHO. Therefore, in the present study, we attempted to clarify specific ET_AR signaling cascades, which were activated in an expression-level dependent manner, with special attention to G_{12} protein, NHE, and p38MAPK.

It has been reported that stimulation of GPCRs coupled to G_q (31), G_s (9), and G_{12} (32) activate NHE. Notably, ET_AR can be coupled with these types of G proteins. To characterize intracellular mechanisms underlying NHE activation by ET_AR, we employed the Cytosensor™ microphysiometer, because the machine is

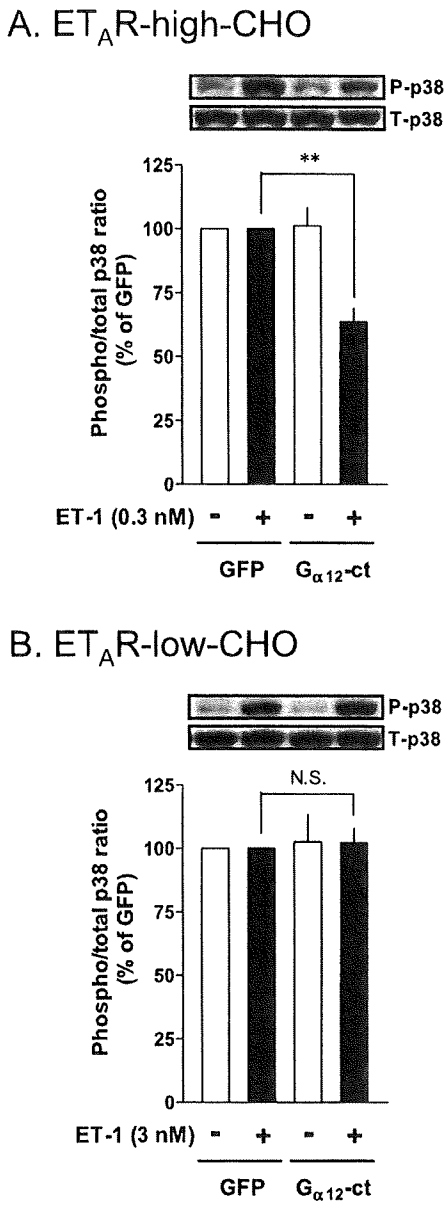

Fig. 9. Effects of introducing GFP and $G_{\alpha 12}$-ct along with GFP by adenovirus infection on p38MAPK phosphorylation in response to 30-min exposure to 0.3 nM ET-1 in ET_AR-high-CHO (A) and 10-min exposure to 3 nM ET-1 in ET_AR-low-CHO (B). Data are presented as means ± S.E.M. of the results obtained from 6 experiments (**$P<0.01$; N.S., not significant between the indicated columns).

reported to be a valuable tool for evaluation of signaling molecules regulating NHE function (23). Functional study with this instrument showed that stimulation of ET_AR induced an increase in ECAR in both ET_AR-high-CHO and ET_AR-low-CHO. The ECAR responses to ET-1 in these cells were considered to be mediated solely by NHE1, since the responses were suppressed by EIPA that shows higher selectivity for NHE1 rather than other members of an NHE family (20).

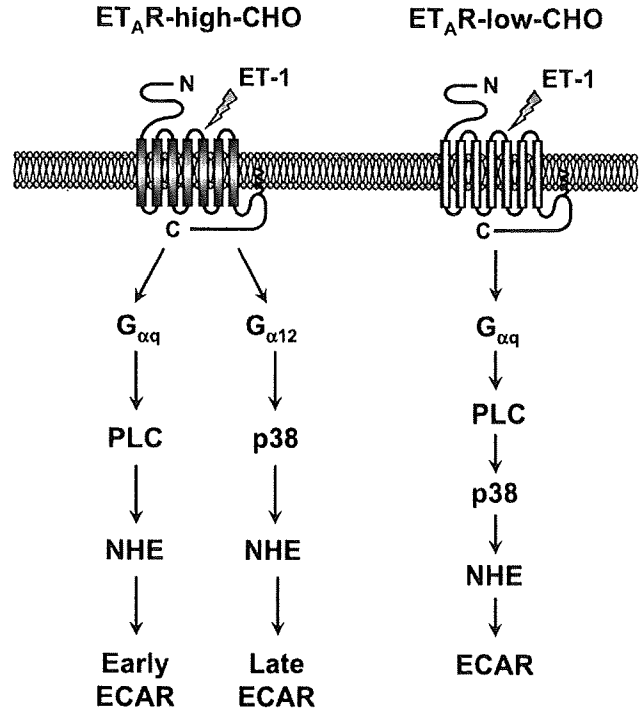

Fig. 10. Multiple signaling pathways utilized by human ET_AR. In ET_AR-high-CHO, ET-1 activates $G_{\alpha q/11}$/PLC/NHE and $G_{\alpha 12}$/p38MAPK/NHE cascades, leading to an increase in ECAR. The involvement of these pathways in the ECAR response to ET-1 varies with time. In ET_AR-low-CHO, ET-1 increases ECAR predominantly via activation of the $G_{\alpha q/11}$/PLC/p38MAPK/NHE pathway.

To clarify molecular mechanisms for ET_AR-mediated NHE activation, real-time analyses together with functional studies using inhibitors for $G_{q/11}$, PLC, and p38MAPK were carried out. This approach has revealed that there is a marked difference in ET_AR signaling involved in NHE activation between ET_AR-high-CHO and ET_AR-low-CHO. In ET_AR-high-CHO, both the $G_{q/11}$/PLC-dependent, p38MAPK-independent pathway and the $G_{q/11}$/PLC-independent, p38MAPK-dependent pathway were involved in the ECAR responses to ET-1, but the contribution of these pathways to the ECAR response varied with time. In contrast, in ET_AR-low-CHO, a unique pathway was found to be predominant, which is $G_{q/11}$/PLC-dependent and p38MAPK-dependent. The possible candidates for the G_q/PLC-independent response observed in ET_AR-high-CHO are G_s- and G_{12}-dependent pathways. However, the involvement of G_s can be ruled out by the result that the ET-1–induced increase in ECAR was unaffected by a G_s inhibitor, NF449 (24), and an AC inhibitor, 2',5'-dideoxyadenosine, which blocks the augmentation of ECAR mediated via the G_s-coupled β_3-AR (9). These results raised the possibility that ET_AR essentially couples to $G_{q/11}$ protein but that excessive receptor expression results in further

coupling of the receptor to other G proteins, possibly G_{12}, in addition to $G_{q/11}$.

The difference in receptor density is also reported to affect the extent of p38MAPK activation by GPCRs. That is, a comparative study with CHO cells stably expressing mouse β_3-ARs at high and low levels has shown that the maximum phosphorylation of p38MAPK mediated via β_3-ARs in low-expressor was larger than that in high-expressor (9). In contrast to β_3-AR, the maximal level of p38MAPK phosphorylation induced by ET-1 in ET_AR-high-CHO was approximately 2-times higher than that in ET_AR-low-CHO. These findings clearly indicate that the correlation between the degree of p38MAPK phosphorylation and receptor expression level is dependent on the types of GPCRs or G proteins specifically coupled to the receptors. Interestingly, Western blot analysis has provided evidence that activation of p38MAPK triggered by ET-1 was mainly mediated via G_{12} in ET_AR-high-CHO but via $G_{q/11}$/PLC in ET_AR-low-CHO. This implies that G_{12} protein would be responsible for the ET-1–induced, p38MAPK-dependent increase in ECAR in ET_AR-high-CHO, while there is no evidence to suggest the involvement of G_{12} in the ECAR response to ET-1 in ET_AR-low-CHO. Unfortunately, a functional approach with combination of Cytosensor™ and adenovirus to inhibit G_{12} is unavailable for demonstrating G_{12} contribution to the ET-1–induced increase in ECAR estimated on the basis of basal ECAR, since it is very difficult to rule out the possibility that inhibition of G_{12} by the adenovirus affects basal ECAR.

In summary, the present study showed that a difference in expression level of human ET_AR results in a multiplicity of receptor signaling as shown in Fig. 10. The pharmacological evidence in the present study allows the following conclusion to be reached concerning the signaling cascades involved in the ECAR response to ET-1: the response in ET_AR-low-CHO is mediated via the $G_{q/11}$/PLC/p38MAPK/NHE pathway, while the response in ET_AR-high-CHO is mediated via either the $G_{q/11}$/PLC/NHE cascade or the G_{12} /p38MAPK/NHE cascade. In addition, both p38MAPK and NHE participate in a sustained increase in $[Ca^{2+}]_i$ triggered by ET-1. These results, taken together with previous reports indicating the involvement of G_{12} in the ET_AR-mediated sustained $[Ca^{2+}]_i$ increase (1, 2), suggest that G_{12}-dependent p38MAPK activation is required for the sustained Ca^{2+} response to ET-1. With regard to the pathophysiological relevance of changes in receptor expression level to diseases, evidence has accumulated to indicate that the up-regulation of ET_AR occurs in various cardiovascular disorders such as ischemic cardiomyopathy (33), hypoxia (34), diabetes mellitus (35), and renal failure (36). Therefore, alternations in receptor signaling associated with changes in receptor density may be important as a key pathophysiological process responsible for these diseases.

Acknowledgments

We thank Dr. Hitoshi Kurose (Kyushu University, Fukuoka) for kindly donating recombinant adenoviruses. We also thank Astellas Pharma, Inc. (Tokyo) for generously providing YM-254890. This study was supported in part by Grants-in-Aids for Young Scientific Research (B) from the Ministry of Education, Culture, Sports, Science, and Technology (MEXT), Japan (T.H.) and for Scientific Research (B) from Japan Society for the Promotion of Science (JSPS) (S.M.). It was also supported in part by grants from Smoking Research Foundation of Japan (S.M.), Suzuken Memorial Foundation (T.H.), Northern Advancement Center for Science and Technology (NOASTEC) (T.H.), the Pharmacological Research Foundation, Tokyo (T.H.), the Akiyama Life Science Foundation (T.H.), and Actelion Pharmaceuticals Japan, Ltd. (T.H.).

References

1 Kawanabe Y, Okamoto Y, Miwa S, Hashimoto N, Masaki T. Molecular mechanisms for the activation of voltage-independent Ca^{2+} channels by endothelin-1 in Chinese hamster ovary cells stably expressing human $endothelin_A$ receptors. Mol Pharmacol. 2002;62:75–80.

2 Miwa S, Kawanabe Y, Okamoto Y, Masaki T. Ca^{2+} entry channels involved in endothelin-1-induced contractions of vascular smooth muscle cells. J Smooth Muscle Res. 2005;41:61–75.

3 Enoki T, Miwa S, Sakamoto A, Minowa T, Komuro T, Kobayashi S, et al. Long-lasting activation of cation current by low concentration of endothelin-1 in mouse fibroblasts and smooth muscle cells of rabbit aorta. Br J Pharmacol. 1995;115: 479–485.

4 Iwamuro Y, Miwa S, Minowa T, Enoki T, Zhang XF, Ishikawa M, et al. Activation of two types of Ca^{2+}-permeable nonselective cation channel by endothelin-1 in A7r5 cells. Br J Pharmacol. 1998;124:1541–1549.

5 Iwamuro Y, Miwa S, Zhang XF, Minowa T, Enoki T, Okamoto Y, et al. Activation of three types of voltage-independent Ca^{2+} channel in A7r5 cells by endothelin-1 as revealed by a novel Ca^{2+} channel blocker LOE 908. Br J Pharmacol. 1999;126:1107–1114.

6 Horinouchi T, Nishimoto A, Nishiya T, Lu L, Kajita E, Miwa S. Endothelin-1 decreases $[Ca^{2+}]_i$ via Na^+/Ca^{2+} exchanger in CHO cells stably expressing endothelin ET_A receptor. Eur J Pharmacol. 2007;566:28–33.

7 Horinouchi T, Miyake Y, Nishiya T, Nishimoto A, Morishima S, Muramatsu I, et al. Functional role of Na^+/H^+ exchanger in Ca^{2+} influx mediated via human endothelin type A receptor stably expressed in Chinese hamster ovary cells. J Pharmacol Sci. 2008;107:456–459.

8 Michel MC, Alewijnse AE. Ligand-directed signaling: 50 ways to find a lover. Mol Pharmacol. 2007;72:1097–1099.

9 Sato M, Horinouchi T, Hutchinson DS, Evans BA, Summers RJ. Ligand-directed signaling at the β_3-adrenoceptor produced by 3-(2-ethylphenoxy)-1-[(1,S)-1,2,3,4-tetrahydronapth-1-ylamino]-

2S-2-propanol oxalate (SR59230A) relative to receptor agonists. Mol Pharmacol. 2007;72:1359–1368.
10 Kenakin T. Differences between natural and recombinant G protein-coupled receptor systems with varying receptor/G protein stoichiometry. Trends Pharmacol Sci. 1997;18:456–464.
11 Kenakin T. Functional selectivity through protean and biased agonism: who steers the ship? Mol Pharmacol. 2007;72:1393–1401.
12 Urban JD, Clarke WP, von Zastrow M, Nichols DE, Kobilka B, Weinstein H, et al. Functional selectivity and classical concepts of quantitative pharmacology. J Pharmacol Exp Ther. 2007;320:1–13.
13 Cordeaux Y, Briddon SJ, Megson AE, McDonnell J, Dickenson JM, Hill SJ. Influence of receptor number on functional responses elicited by agonists acting at the human adenosine A_1 receptor: evidence for signaling pathway-dependent changes in agonist potency and relative intrinsic activity. Mol Pharmacol. 2000;58:1075–1084.
14 Wu-Wong JR, Chiou WJ, Magnuson SR, Opgenorth TJ. Endothelin receptor in human astrocytoma U373MG cells: binding, dissociation, receptor internalization. J Pharmacol Exp Ther. 1995;274:499–507.
15 Bradford MM. A rapid and sensitive method for the quantitation of microgram quantities of protein utilizing the principle of protein-dye binding. Anal Biochem. 1976;72:248–254.
16 Arai K, Maruyama Y, Nishida M, Tanabe S, Takagahara S, Kozasa T, et al. Differential requirement of $G\alpha_{12}$, $G\alpha_{13}$, $G\alpha_q$, and $G\beta\gamma$ for endothelin-1-induced c-Jun NH_2-terminal kinase and extracellular signal-regulated kinase activation. Mol Pharmacol. 2003;63:478–488.
17 Horinouchi T, Miyake Y, Nishiya T, Nishimoto A, Yorozu S, Jinno A, et al. Characterization of noradrenaline-induced increases in intracellular Ca^{2+} levels in Chinese hamster ovary cells stably expressing human α_{1A}-adrenoceptor. J Pharmacol Sci. 2007;105:103–111.
18 Takasaki J, Saito T, Taniguchi M, Kawasaki T, Moritani Y, Hayashi K, et al. A novel $G_{\alpha q/11}$-selective inhibitor. J Biol Chem. 2004;279:47438–47445.
19 Kristiansen K. Molecular mechanisms of ligand binding, signaling, and regulation within the superfamily of G-protein-coupled receptors: molecular modeling and mutagenesis approaches to receptor structure and function. Pharmacol Ther. 2004;103:21–80.
20 Putney LK, Denker SP, Barber DL. The changing face of the Na^+/H^+ exchanger, NHE1: structure, regulation, and cellular actions. Annu Rev Pharmacol Toxicol. 2002;42:527–552.
21 Lee HM, Won KJ, Kim J, Park HJ, Kim HJ, Roh HY, et al. Endothelin-1 induces contraction via a Syk-mediated p38 mitogen-activated protein kinase pathway in rat aortic smooth muscle. J Pharmacol Sci. 2007;103:427–433.
22 Kim B, Kim J, Bae YM, Cho SI, Kwon SC, Jung JY, et al. p38 mitogen-activated protein kinase contributes to the diminished aortic contraction by endothelin-1 in DOCA-salt hypertensive rats. Hypertension. 2004;43:1086–1091.
23 McConnell HM, Owicki JC, Parce JW, Miller DL, Baxter GT, Wada HG, et al. The cytosensor microphysiometer: biological applications of silicon technology. Science. 1992;257:1906–1912.
24 Hohenegger M, Waldhoer M, Beindl W, Böing B, Kreimeyer A, Nickel P, et al. $G_{s\alpha}$-selective G protein antagonists. Proc Natl Acad Sci U S A. 1998;95:346–351.
25 Eason M, Kurose H, Holt B, Raymond J, Liggett S. Simultaneous coupling of α_2-adrenergic receptors to two G-proteins with opposing effects. Subtype-selective coupling of α_2C10, α_2C4, and α_2C2 adrenergic receptors to G_i and G_s. J Biol Chem. 1992;267:15795–15801.
26 Perez DM, Karnik SS. Multiple signaling states of G-protein-coupled receptors. Pharmacol Rev. 2005;57:147–161.
27 Venkatachalam K, van Rossum DB, Patterson RL, Ma HT, Gill DL. The cellular and molecular basis of store-operated calcium entry. Nat Cell Biol. 2002;4:E263–E272.
28 Spassova MA, Soboloff J, He LP, Hewavitharana T, Xu W, Venkatachalam K, et al. Calcium entry mediated by SOCs and TRP channels: variations and enigma. Biochim Biophys Acta. 2004;1742:9–20.
29 Barritt GJ. Receptor-activated Ca^{2+} inflow in animal cells: a variety of pathways tailored to meet different intracellular Ca^{2+} signalling requirements. Biochem J. 1999;337:153–169.
30 McFadzean I, Gibson A. The developing relationship between receptor-operated and store-operated calcium channels in smooth muscle. Br J Pharmacol. 2002;135:1–13.
31 Taniguchi T, Inagaki R, Suzuki F, Muramatsu I. Rapid acid extrusion response triggered by α_1 adrenoceptor in CHO cells. J Physiol. 2001;535:107–113.
32 Orlowski J, Grinstein S. Na^+/H^+ exchangers of mammalian cells. J Biol Chem. 1997;272:22373–22376.
33 Serneri G, Cecioni I, Vanni S, Paniccia R, Bandinelli B, Vetere A, et al. Selective upregulation of cardiac endothelin system in patients with ischemic but not idiopathic dilated cardiomyopathy: endothelin-1 system in the human failing heart. Circ Res. 2000;86:377–385.
34 Chen Y, Tipoe G, Liong E, Leung S, Lam S, Iwase R, et al. Chronic hypoxia enhances endothelin-1-induced intracellular calcium elevation in rat carotid body chemoreceptors and up-regulates ET_A receptor expression. Pflugers Arch. 2002;443:565–573.
35 Su W, Dai D, Liu H, Na T, Dai Y. Upregulated endothelin system in diabetic vascular dysfunction and early retinopathy is reversed by CPU0213 and total triterpene acids from Fructus Corni. Clin Exp Pharmacol Physiol. 2007;34:1228–1233.
36 Roubert P, Gillard-Roubert V, Pourmarin L, Cornet S, Guilmard C, Plas P, et al. Endothelin receptor subtypes A and B are up-regulated in an experimental model of acute renal failure. Mol Pharmacol. 1994;45:182–188.

International Immunology, Vol. 21, No. 11, pp. 1263–1268
doi:10.1093/intimm/dxp092

Histidine decarboxylase but not histamine receptor 1 or 2 deficiency protects from K/BxN serum-induced arthritis

Narendiran Rajasekaran[1,6], Samuel Solomon[2], Takeshi Watanabe[3], Hiroshi Ohtsu[4], Mieczyslaw Gajda[5], Rolf Bräuer[5] and **Harald Illges[1]**

[1]Immunology and Cell Biology, University of Applied Sciences Bonn-Rhein-Sieg, von-Liebig-Strasse 20, D-53359 Rheinbach, Germany
[2]The Biomedical Research Centre, University of British Columbia, 2222 Health Sciences Mall, Vancouver, BCV6T 1Z3, Canada
[3]Department of Molecular Immunology, Medical Institute of Bioregulation, Kyushu University, 3-1-1 Maidashi, Higashi-ku, Fukuoka, Fukuoka 812-8582, Japan
[4]Graduate School of Engineering, Applied Quantum Medical Engineering, Tohoku University, Aza-Aoba 6-6-01, Aramaki, Aoba-ku, Sendai, 980-8579, Japan
[5]Institute of Pathology, University Hospital Jena, Ziegelmühlenweg 1, D-07740 Jena, Germany

[6]Present address: Department of Pediatrics, Stanford University, Stanford, CA 94305, USA

Keywords: histamine receptor, histidine decarboxylase, K/BxN mouse model

Abstract

Serum transfer from arthritic K/BxN mice into naive animals results in arthritis. Mast cells have been shown to be essential since mice lacking these cell type do not develop arthritis upon serum injection. Mast cell function depends on the release of granules filled with mediators such as histamine. Mice deficient in histidine decarboxylase ($HDC^{-/-}$) that do not produce histamine and mice deficient for histamine receptor 1 ($H1R^{-/-}$) or histamine receptor 2 ($H2R^{-/-}$) were injected with arthritogenic sera from the K/BxN mice, and the progression of arthritis was observed through the next 2 weeks. $HDC^{-/-}$ mice that are histamine free developed a milder form of arthritis in comparison with the wild-type controls. In both receptor-deficient mice as well as in wild-type controls, the onset and severity of clinical arthritis and ankle thickening occurred during day 1 to 3. These results indicate that histamine is required but not indispensable for the development of serum-induced arthritis and histamine receptors other than those studied here may be involved.

Introduction

Crossing the TCR Vβ6 transgenic KRN mouse strain with the NOD/Lt mouse results in F1 mice (K/BxN) that develop arthritis spontaneously (1). In the arthritic mice, autoantibodies are produced against the ubiquitous glycolytic enzyme glucose-6-phosphate isomerase dependent on both the TCR transgene and the NOD-derived IAg^7 molecule (2). When sera or purified antibodies from the K/BxN mice are transferred to normal mice, a transient form of the arthritis develops. This serum transfer model has been used to identify various cellular and molecular components involved in the induction of inflammation. Neutrophils, mast cells and macrophages have been identified as important cellular factors required for disease development (3–5). Further, the arthritogenic antibodies act through the FcγRIII receptors and C5a and the alternate complement network is essential for the development of the disease (6, 7).

Mast cell-deficient mice were completely protected against K/BxN serum-induced arthritis (5) and mast cells in the synovium were found to degranulate within an hour of serum transfer into naive mice. Mast cell reconstitution of mast cell-deficient mice fully restored arthritis (8). Mast cell stabilization by compounds salbutamol or cromolyn within 24 h of sera injection prevented angiogenesis, pannus formation and joint destruction (8). Mast cells, thus, play an important role in the initiation of the disease. Mast cells secrete a variety of potential inflammatory mediators like histamine, leukotrienes, proteinases, heparin, vascular endothelial growth factor (VEGF) and various other cytokines

Correspondence to: H. Illges; E-mail: harald.illges@fh-brs.de

Transmitting editor: A. Radbruch

Received 16 April 2009, *accepted* 19 August 2009

Advance Access publication 17 September 2009

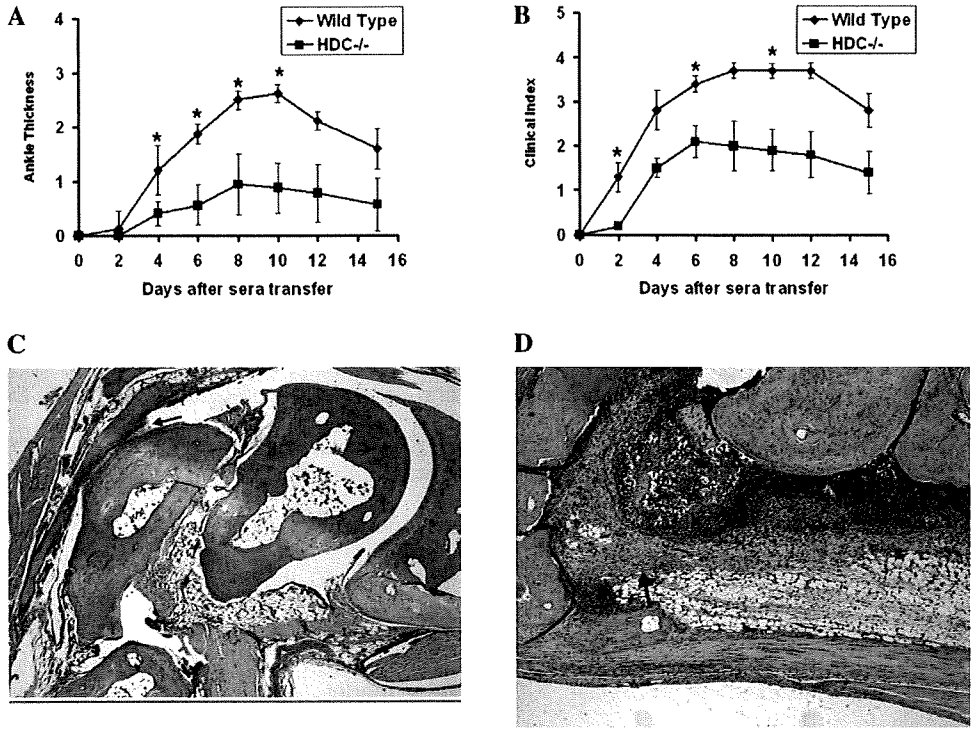

Fig. 1. HDC$^{-/-}$ mice showed reduced severity of K/BxN serum-induced arthritis. HDC$^{-/-}$ mice and wild-type controls were treated with 200 μl of K/BxN serum and arthritis evaluated by measuring ankle thickness (A) and clinical index (B) as given in Methods. Shown here is the difference in ankle thickness and clinical index between each time point and day 0. Data are expressed as mean ± SEM ($n > 5$). The HDC$^{-/-}$ mice showed significantly reduced severity of arthritis when compared with the wild-type controls ($P < 0.05$ between day 4 and 15). Mice sacrificed on day 4 of arthritis were assessed histologically. Ankle sections of HDC$^{-/-}$ mice (C) showed reduced degrees of synovial inflammation and pannus formation (arrow) when compared with the wild-type controls (D) (H & E, ×40).

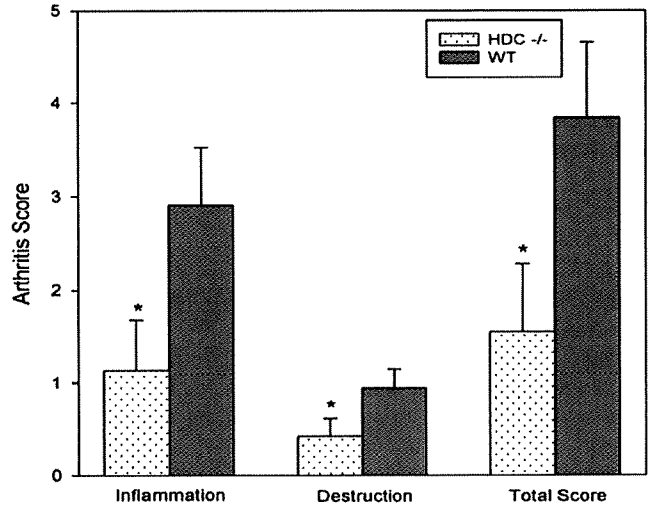

Fig. 2. Histological evaluation of inflammation and joint destruction within hind paws and ankles 4 days after K/BxN serum transfer. In comparison with wild-type controls (WT), the severity of arthritis in HDC$^{-/-}$ mice is significantly decreased; *$P < 0.05$, $n > 5$.

including tumor necrosis factor-α (TNF-α) (9). The two important mediators histamine and TNF-α are capable of being released immediately after mast cell activation from preformed granules. Investigating the role histamine and its receptors during arthritis development will give us an insight into how mast cells mediate development of arthritis.

Histamine, a mediator of allergic reactions, is contained in the mast cell granules and is released during inflammation when mast cells are activated either by cross-linking the FcεRI receptors or FcγRIII receptors (10, 11). Histamine acts as a vasodilator and chemoattractant through its receptors. Four receptors of histamine, H1–H4, have been identified so far. These receptors differ in their tissue distribution and mediate different roles in inflammation depending on the location of the inflammation and the surrounding inflammatory milieu. The H1 receptor mediates endothelial cell and smooth muscle responses to histamine. Activation of the H1 receptor causes bronchoconstriction, vasodilatation and increased vascular permeability (12–14). H2 receptors on vascular smooth muscle cells also mediate vasodilation (15).

To analyze whether histamine has a role in this disease model, we induced arthritis in histidine decarboxylase-deficient (HDC$^{-/-}$) mice. Histidine decarboxylase is an essential enzyme in histamine biosynthesis and forms histamine from L-histidine and therefore, the HDC$^{-/-}$ mice do not make histamine. To further investigate if histamine's effect on arthritis is mediated through its receptors 1 and 2, we did K/BxN serum transfer in histamine receptor 1-deficient (H1R$^{-/-}$) and histamine receptor 2-deficient (H2R$^{-/-}$) mice.

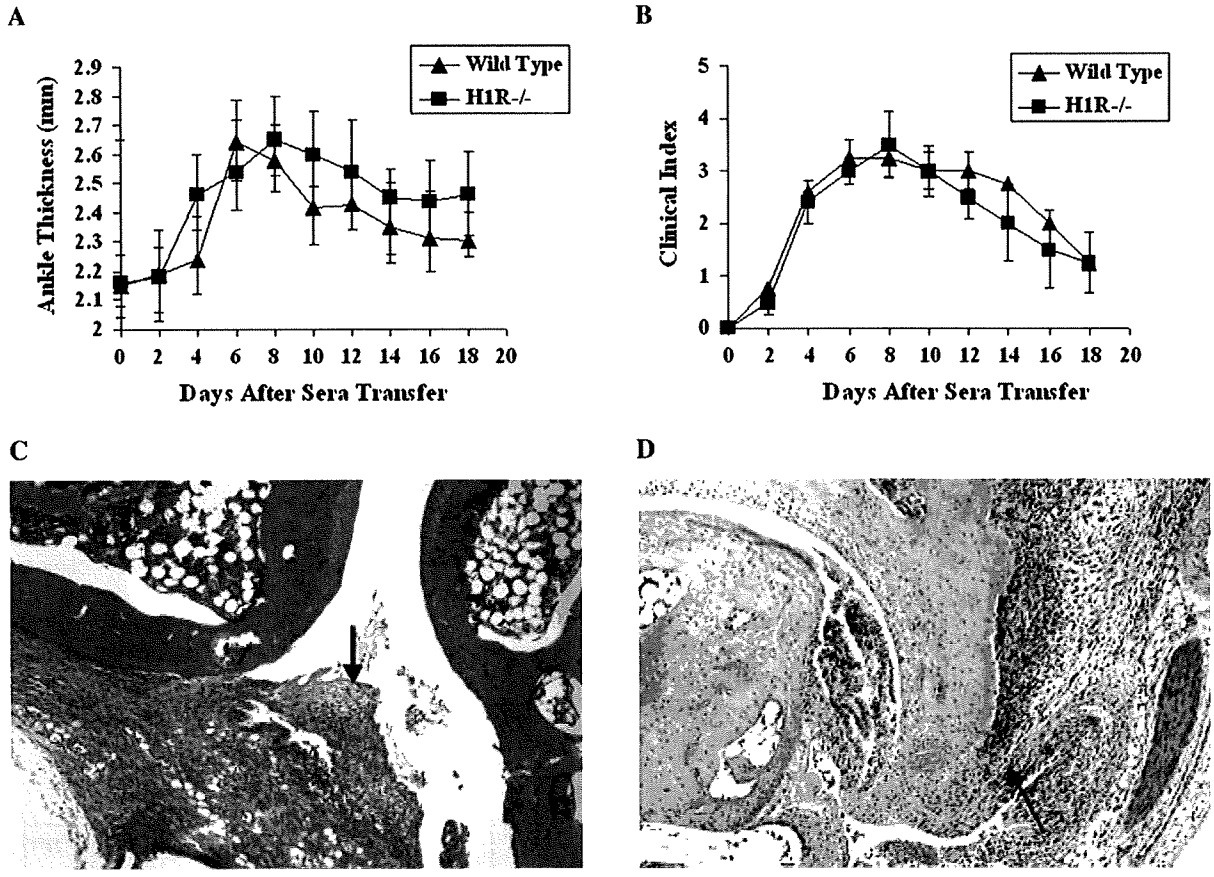

Fig. 3. $H1R^{-/-}$ mice were not protected against K/BxN serum-induced arthritis. $H1R^{-/-}$ mice and wild-type controls were treated with 200 µl of K/BxN serum and arthritis evaluated by measuring ankle thickness (A) and clinical index (B) as given in Methods. Data are expressed as mean ± SEM ($n > 5$). There were no differences in ankle thickness or clinical index scores between the two groups. Mice sacrificed on day 4 of arthritis were assessed histologically. Ankle sections of $H1R^{-/-}$ mice (C) showing synovial inflammation and pannus formation (arrow) similar as in wild-type controls (D) (H & E, ×40).

Methods

Experimental animals

The KRN transgenic mice were a kind gift from D. Mathis and C. Benoist (IGMBC, Strasbourg, France) (1). C57BL/6 (B6) mice and NOD/Lt mice were obtained from our animal facility and were maintained under pathogen-free conditions. $HDC^{-/-}$ mice were obtained from Prof. Hiroshi Ohtsu (16). $H1R^{-/-}$ and $H2R^{-/-}$ mice were obtained from Prof. Takeshi Watanabe (17, 18). The KRN and K/BxN strains were bred as described earlier (7).

Induction of arthritis by K/BxN serum transfer and arthritis assessment

Arthritis was induced in the recipient mice by an intraperitoneal injection of 200 µl of the K/BxN sera (7). Increase in ankle thickening was measured using a micrometer (Hann and Kolb, model no. 33185). Ankle thickness, the summed average of the thickness of the four limbs per mice, was expressed in millimeters. Clinical index score, independent on the number of ankles affected, was measured in a scale varying from 0 to 4. Histology was performed and evaluated in a blinded manner as described (19).

Statistical analysis

The data were expressed as the means ± SEMs. Statistical analysis was performed with SPSS for Windows version 10.0 (SPSS, Chicago, IL, USA). Data were analyzed with the Mann–Whitney *U*-test. For each test, P values ≤ 0.05 were considered significant.

Histochemistry

Mice were sacrificed by cervical dislocation. Ankle joints were removed, skinned and prepared by fixing for 24 h in 4% phosphate-buffered formaldehyde. Fixed joints were decalcified by treatment with Osteosoft (Merck KGaA, Darmstadt, Germany) for 1 week. Samples were then washed with PBS, dehydrated with a series of ethanol washes (50% ethanol, followed by 70% ethanol) and embedded in paraffin. Sections of tissue 4 µm thick were cut and stained with hematoxylin and eosin (H & E). Four sections per joint were examined and scored in a blinded manner for the extent of inflammation and joint destruction. The extent of joint inflammation was defined by synovial hyperplasia and degree of infiltration of the synovial membrane by granulocytes and scored as follows: 0, no infiltration; 1, mild infiltration; 2, moderate infiltration and 3, severe infiltration. The extent of

the damage to cartilage and bone structures (structural bone defects and cartilage cell necrosis) was evaluated on a scale of 0–3, where 0—no damage, 1—mild destruction, 2—medium damage of bony matrix and 3—severe damage of bone (extensive area of destruction, deep invasive destructions of bone).

Results

To elucidate the role of histamine in serum-induced arthritis, we injected 200 μl K/BxN sera intraperitoneally into $HDC^{-/-}$ mice and C57Bl/6 wild-type controls. Onset and progression of arthritis was observed through the next 2 weeks determining ankle thickness by caliper measurement and a clinical determining the numbers of affected joints. The onset of clinical arthritis and ankle thickening occurred around 24–48 h in both $HDC^{-/-}$ and control mice, but $HDC^{-/-}$ mice, which are not able to produce histamine, developed a milder form of arthritis when compared with the wild-type mice (Fig. 1A and B). Inflammation was assessed histologically from ankle sections of mice sacrificed on different days during the course of arthritis. Histological examination of the $HDC^{-/-}$ mice showed a reduced severity of arthritis (synovial inflammation, pannus formation; Fig. 1C) when compared with the wild-type controls (Fig. 1D). Statistical analysis showed significant differences in both ankle thickness (days 4, 6, 8 and 10) and clinical index (days 2, 6, 8 and 10). Together, this shows that absence of histamine ameliorates serum-induced arthritis but does not protect the mice from arthritis.

To determine the strength of the rheumatic disease in our experimental mice, we examined four sections per joint and scored in a blinded manner for the extent of inflammation (synovial hyperplasia, cellular infiltration of synovial tissue) and joint destruction (pannus formation, cartilage and bone degradation). The results of this analysis (Fig. 2) show that both inflammation and joint destruction are significantly reduced in the absence of histidine decarboxylase (HDC) in the deficient mice.

In order to elucidate which receptors are involved in mediating the histamine effects on arthritis, K/BxN sera were injected into $H1R^{-/-}$ or $H2R^{-/-}$ mice and C57Bl/6 wild-type controls. Mice were experimentally treated and analyzed in the same way as described above for the HDC-deficient animals. There were no detectable differences in the onset of ankle thickening (Figs 3A and 4A), clinical arthritis (Figs 3B and 4B) and histological severity of arthritis (Fig. 3C and D and Fig. 4C and D) between both types of histamine receptor-deficient and control mice. Our results indicate that both examined histamine receptors have no essential role in this serum-induced arthritis model.

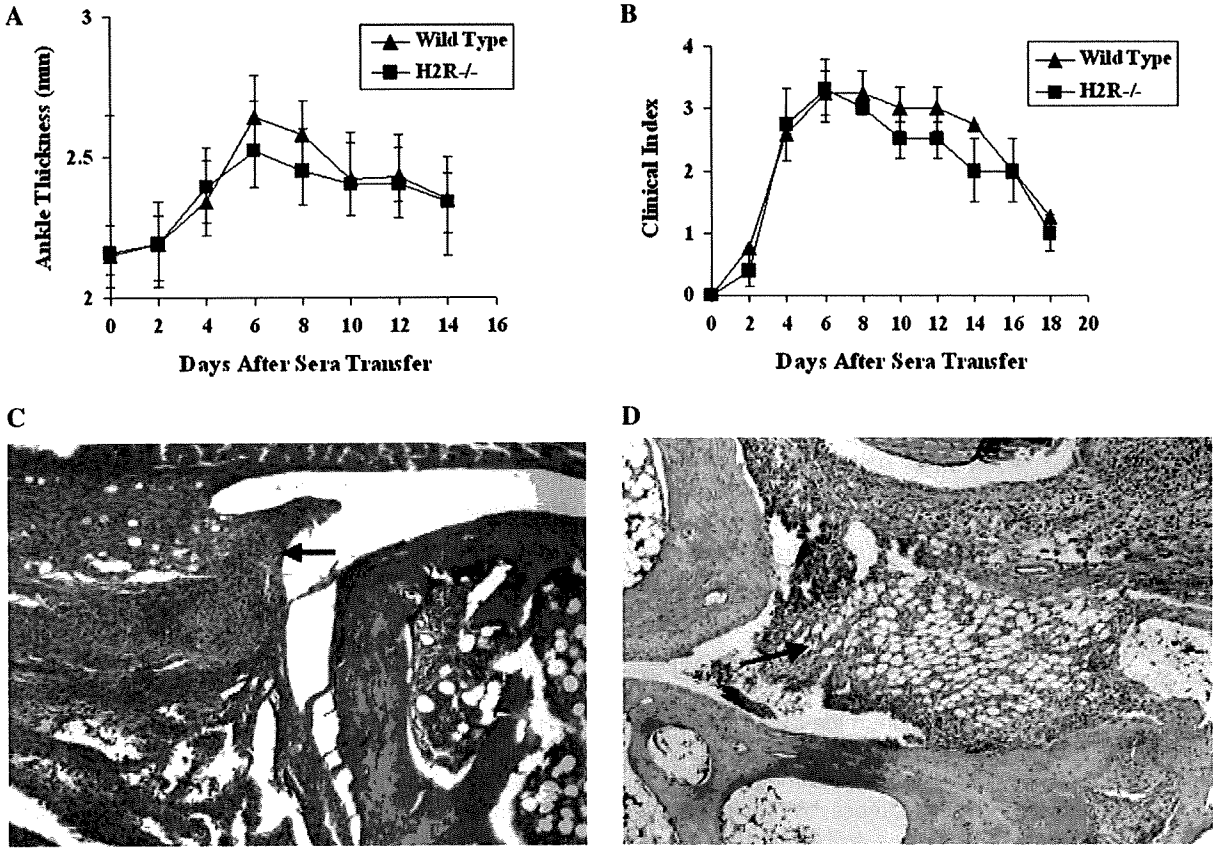

Fig. 4. Histamine receptor 2 is not required for K/BxN serum-induced arthritis. $H2R^{-/-}$ mice when given 200 μl of K/BxN serum developed arthritis similar to the wild-type controls. This was shown in the ankle thickness (A) and clinical index scores (B) measured as given in Methods. Data are expressed as mean ± SEM ($n > 5$). Serum transferred mice sacrificed on day 4 of arthritis were assessed histologically. Ankle sections from $H2R^{-/-}$ mice (C) showed similar degrees of synovitis and joint destruction (arrow) when compared with the wild-type control (D) (H & E, ×40).

Discussion

From the above experiments, we can conclude that histamine is essential for arthritis development but not indispensable. Alternatively, mediators other than histamine that promote mast cell activity might be important. In this context, it was already demonstrated that VEGF, which promotes vasodilatation and angiogenesis, is essential for arthritis development in the K/BxN model (20). Another important candidate is TNF-α. Like histamine, TNF-α is released by mast cells as a preformed mediator but is also synthesized later for a sustained release (21). TNF-α is also capable of mediating vasodilatation (22, 23). Mast cell-secreted TNF-α has been shown to play an important role in immune complex-mediated diseases. The K/BxN serum-induced arthritis is basically an immune complex-mediated type III hypersensitivity reaction. In a model of immune complex-induced inflammation of the peritoneal cavity, TNF-α secreted by mast cells was shown to augment neutrophil emigration (24). In a mice model of rheumatoid factor-mediated skin vasculitis, mast cells were essential for triggering vasculitis and mast cells mediated their action through FcγRIII receptor and TNF-α (25). Further investigations are being carried out to find if TNF-α is also an important mediator of mast cell effects in this model of arthritis.

Histamine mediates its action through a variety of four different receptors (H1–H4) (26–28). These receptors differ in their tissue distribution (26, 29). They mediate different roles in inflammation depending on the location of the inflammation and the surrounding inflammatory milieu (27). Though H1 and H2 receptors do not have a role in K/BxN serum-induced arthritis, histamine may still mediate its effects through the other two receptors H3 and H4. The expression of histamine receptor 4 in the synovial cells from rheumatoid arthritis patients has been recently shown (30, 31). Further, in the absence of one of the receptors in the knockout mice, its functions may be compensated by the other receptors. Another possibility is that absence of both the H1 and H2 receptors may be required to show a pronounced effect on the disease.

In conclusion, our study shows that histamine is required for the development of K/BxN serum-induced arthritis. However, the role of histamine receptors is unclear and the involvement of other receptors of histamine like H3 and H4 need to be investigated.

Funding

EU grant (MRTN-CT-2004-005693); Deutsche Forschungsgemeinschaft (BR 1372/9).

Acknowledgements

The authors appreciate the excellent technical support of Cornelia Hüttich.
Conflict of Interest: The authors declare that they have no conflict of interest.

Abbreviations

HDC	histidine decarboxylase
$HDC^{-/-}$	histidine decarboxylase-deficient
$H1R^{-/-}$	histamine receptor 1-deficient
$H2R^{-/-}$	histamine receptor 2-deficient
H & E	hematoxylin and eosin
TNF-α	tumor necrosis factor-α
VEGF	vascular endothelial growth factor

References

1 Kouskoff, V., Korganow, A. S., Duchatelle, V., Degott, C., Benoist, C. and Mathis, D. 1996. Organ-specific disease provoked by systemic autoimmunity. *Cell* 87:811.
2 Matsumoto, I., Staub, A., Benoist, C. and Mathis, D. 1999. Arthritis provoked by linked T and B cell recognition of a glycolytic enzyme. *Science* 286:1732.
3 Wipke, B. T. and Allen, P. M. 2001. Essential role of neutrophils in the initiation and progression of a murine model of rheumatoid arthritis. *J. Immunol.* 167:1601.
4 Wipke, B. T., Wang, Z., Nagengast, W., Reichert, D. E. and Allen, P. M. 2004. Staging the initiation of autoantibody-induced arthritis: a critical role for immune complexes. *J. Immunol.* 172:7694.
5 Lee, D. M., Friend, D. S., Gurish, M. F., Benoist, C., Mathis, D. and Brenner, M. B. 2002. Mast cells: a cellular link between autoantibodies and inflammatory arthritis. *Science* 297:1689.
6 Ji, H., Ohmura, K., Mahmood, U. *et al.* 2002. Arthritis critically dependent on innate immune system players. *Immunity* 16:157.
7 Solomon, S., Kolb, C., Mohanty, S. *et al.* 2002. Transmission of antibody-induced arthritis is independent of complement component 4 (C4) and the complement receptors 1 and 2 (CD21/35). *Eur. J. Immunol.* 32:644.
8 Kneilling, M., Hultner, L., Pichler, B. J. *et al.* 2007. Targeted mast cell silencing protects against joint destruction and angiogenesis in experimental arthritis in mice. *Arthritis Rheum.* 56:1806.
9 Wooley, D. E. 1995. Mast cells in the rheumatoid lesion—ringleaders or innocent bystanders? *Ann. Rheum. Dis.* 54:533.
10 Baumann, U., Chouchakova, N., Gewecke, B. *et al.* 2001. Distinct tissue site-specific requirements of mast cells and complement components C3/C5a receptor in IgG immune complex-induced injury of skin and lung. *J. Immunol.* 167:1022.
11 Baumann, U., Kohl, J., Tschernig, T. *et al.* 2000. A codominant role of Fc gamma RI/III and C5aR in the reverse Arthus reaction. *J. Immunol.* 164:1065.
12 Chiba, S. and Tsukada, M. 1997. Mechanisms for histamine H1 receptor-mediated vasodilation in isolated canine lingual arteries. *Eur. J. Pharmacol.* 329:63.
13 Parsons, G. H., Villablanca, A. C., Brock, J. M. *et al.* 1992. Bronchial vasodilation by histamine in sheep: characterization of receptor subtype. *J. Appl. Physiol.* 72:2090.
14 Dachman, W. D., Bedarida, G., Blaschke, T. F. and Hoffman, B. B. 1994. Histamine-induced venodilation in human beings involves both H1 and H2 receptor subtypes. *J. Allergy Clin. Immunol.* 93:606.
15 Chiba, S. and Tsukada, M. 1991. Histamine-induced vasodilations mediated by H1- and H2-receptors in isolated rat common carotid arteries. *Heart Vessels* 6:185.
16 Ohtsu, H., Tanaka, S., Terui, T. *et al.* 2001. Mice lacking histidine decarboxylase exhibit abnormal mast cells. *FEBS Lett.* 502:53.
17 Inoue, I., Yanai, K., Kitamura, D. *et al.* 1996. Impaired locomotor activity and exploratory behavior in mice lacking histamine H1 receptors. *Proc. Natl Acad. Sci. USA* 93:13316.
18 Kobayashi, T., Tonai, S., Ishihara, Y., Koga, R., Okabe, S. and Watanabe, T. 2000. Abnormal functional and morphological regulation of the gastric mucosa in histamine H2 receptor-deficient mice. *J. Clin. Investig.* 105:1741.
19 Solomon, S., Rajasekaran, N., Jeisy-Walder, E., Snapper, S. B. and Illges, H. 2005. A crucial role for macrophages in the pathology of K/B x N serum-induced arthritis. *Eur. J. Immunol.* 35: 3064.
20 De Bandt, M., Ben Mahdi, M. H., Ollivier, V. *et al.* 2003. Blockade of vascular endothelial growth factor receptor I (VEGF-RI), but not VEGF-RII, suppresses joint destruction in the K/BxN model of rheumatoid arthritis. *J. Immunol.* 171:4853.

21 Gordon, J. R. and Galli, S. J. 1991. Release of both preformed and newly synthesized tumor necrosis factor alpha (TNF-alpha)/cachectin by mouse mast cells stimulated via the Fc epsilon RI. A mechanism for the sustained action of mast cell-derived TNF-alpha during IgE-dependent biological responses. *J. Exp. Med.* 174:103.
22 Hollenberg, S. M., Cunnion, R. E. and Parrillo, J. E. 1991. The effect of tumor necrosis factor on vascular smooth muscle. *In vitro* studies using rat aortic rings. *Chest* 100:1133.
23 Johns, D. G. and Webb, R. C. 1998. TNF-alpha-induced endothelium-independent vasodilation: a role for phospholipase A2-dependent ceramide signaling. *Am. J. Physiol.* 275:H1592.
24 Zhang, Y., Ramos, B. F. and Jakschik, B. A. 1992. Neutrophil recruitment by tumor necrosis factor from mast cells in immune complex peritonitis. *Science* 258:1957.
25 Watanabe, N., Akikusa, B., Park, S. Y. *et al.* 1999. Mast cells induce autoantibody-mediated vasculitis syndrome through tumor necrosis factor production upon triggering Fcgamma receptors. *Blood* 94:3855.
26 Hill, S. J., Ganellin, C. R., Timmerman, H. *et al.* 1997. International Union of Pharmacology. XIII. Classification of histamine receptors. *Pharmacol. Rev.* 49:253.
27 Hill, S. J. 1990. 1990. Distribution, properties, and functional characteristics of three classes of histamine receptor. *Pharmacol. Rev.* 42:45.
28 Del Valle, J. and Gantz, I. 1997. Novel insights into histamine H2 receptor biology. *Am. J. Physiol.* 273:G987.
29 Leurs, R., Smit, M. J. and Timmerman, H. 1995. Molecular pharmacological aspects of histamine receptors. *Pharmacol. Ther.* 66:413.
30 Ikawa, Y., Suzuki, M., Shiono, S. *et al.* 2005. Histamine H4 receptor expression in human synovial cells obtained from patients suffering from rheumatoid arthritis. *Biol. Pharm. Bull.* 28: 2016.
31 Ohki, E., Suzuki, M., Aoe, T., Ikawa, Y., Negishi, E. and Ueno, K. 2007. Expression of histamine H4 receptor in synovial cells from rheumatoid arthritic patients. *Biol. Pharm. Bull.* 30:2217.

Original Paper

International Archives of Allergy and Immunology

Int Arch Allergy Immunol 2009;149(suppl 1):57–60
DOI: 10.1159/000210655

Published online: June 3, 2009

Effects of Nickel on Eosinophil Survival

Kenji Ishihara[a, b, c] Yoshiaki Goi[c] Jang Ja Hong[c, f] Toshio Seyama[f]
Hiroshi Ohtsu[d] Hiroshi Wada[b] Kazuo Ohuchi[c, f] Noriyasu Hirasawa[c, e]

[a]Course for School Nurse Teacher, Faculty of Education, Ibaraki University, Mito, [b]Department of Bioengineering and Robotics, Graduate School of Engineering, [c]Laboratory of Pathophysiological Biochemistry, Graduate School of Pharmaceutical Sciences, [d]Department of Quantum Science and Energy Engineering, Graduate School of Engineering, and [e]Laboratory of Pharmacotherapy of Life-Style Related Diseases, Graduate School of Pharmaceutical Sciences, Tohoku University, Sendai, and [f]Faculty of Pharmacy, Yasuda Women's University, Hiroshima, Japan

Key Words
Eosinophils · Metal · Nickel

Abstract
Background: Accessories, watches, coins and other items containing metal sometimes cause contact dermatitis and metal allergy. Among metals, nickel in alloys is ionized by sweat on the surface of the skin and exhibits particularly marked irritancy and allergenicity. Although eosinophils play important roles in allergy, the effects of nickel on eosinophils have not been elucidated. ***Methods:*** Eosinophils were prepared from the peritoneal cavity in rats immunized with *Ascaris suum* extract. Purified rat eosinophils were incubated in the presence of various kinds of metals including nickel. The viability of eosinophils was analyzed using a flow cytometer. ***Results:*** When rat eosinophils were incubated for 3 days in the presence of nickel chloride at 30–1,000 μM, the viability of eosinophils was decreased in a concentration-dependent manner. Nickel chloride at 300 μM significantly increased the percentage of annexin V^+ PI^- eosinophils. The population of annexin V^+ PI^- eosinophils was also increased by nickel sulfate, cobalt chloride and zinc sulfate. The binding of nickel ions to eosinophils was detected by flow cytometer. ***Conclusions:*** Nickel ions bind to eosinophils and decrease the viability of eosinophils through the induction of apoptosis. Nickel ions may exhibit activity which modifies the function of eosinophils in allergy.

Introduction

Accessories, watches, coins and other items containing metals sometimes cause contact dermatitis and metal allergy [1, 2]. Among metals, nickel in alloys is ionized by sweat on the surface of the skin and is characterized by irritancy and allergenicity. It has been reported that nickel challenge in the dermis of patients with contact allergy by the skin window technique revealed the infiltration of mononuclear cells, basophils and eosinophils [2, 3].

Eosinophils are suggested to play important roles in the pathogenesis of allergic inflammation such as bronchial asthma and atopic dermatitis [4, 5]. In patients suffering from these allergic diseases, the number of eosinophils in the bone marrow, peripheral blood and at inflammatory sites is increased because of their prolonged survival. Recently, it has been reported that asthmatic patients have a higher sensitivity to nickel than normal [6]. However, the effects of nickel on eosinophils have not been elucidated. In this study, therefore, we analyzed the effects of nickel on the viability of eosinophils.

Materials and Methods

Preparation and Culture of Rat Eosinophils

Preparation of rat peritoneal eosinophils was carried out as previously reported [7]. The purity of eosinophils was more than 95%, and the viability was more than 98%. Eosinophils were seed-

KARGER
Fax +41 61 306 12 34
E-Mail karger@karger.ch
www.karger.com

1018–2438/09/1495–0057$26.00/0

Accessible online at:
www.karger.com/iaa

Correspondence to: Dr. Kenji Ishihara
Course for School Nurse Teacher
Faculty of Education, Ibaraki University
2-1-1 Bunkyo, Mito, Ibaraki 310-8512 (Japan)
Tel./Fax +81 29 228 8300, E-Mail ishihara@mx.ibaraki.ac.jp